Paleomagnetic regional survey of late magmatic & sedimentary of the Southern Rehoboth Basement Inlier

Vuong V. Mai

Advisor: David A. D. Evans, Yale University

Second reader: Richard E. Hanson, Texas Christian University

11 May 2021

A Senior Thesis presented to the faculty of the Department of Earth and Planetary Sciences, Yale University, in partial fulfillment of the Bachelor's Degree.

Contents

Abstract

The Rehoboth Basement Inlier (RBI) in present-day Namibia is part of the Kalahari craton that is immediately adjacent to the ca. 550-500 Ma Pan-African Damara Orogen. This study presents a regional paleomagnetic survey of sedimentary and magmatic rocks in this region to explore its spatial evolution during the Meso-Neoproterozoic. Sample suites were taken from mafic dykes near the Klein Aub region in the southwest and redbeds and volcanics of the Doornpoort Formation in the Southeast. Only one of seven dyke sample suites showed interpretable results, while many of the redbeds and volcanics showed a single-component magnetization held primarily by hematite. Our fold test results are suggestive of syn-folding magnetization similar to results from a previous study on rocks of the Aubures Formation in the Konkiep Subprovince. The characteristic direction of this magnetization is similar to the $\sim$1105 Ma Umkondo paleomagnetic poles but distinct from the $\sim$1030-1000 Ma poles. We suggest an age of ca. 1100 Ma for folding of the Doornpoort formation. This would imply that a Mesoproterozoic deformation event was active in the Rehoboth province and that not all fold structures observed in this region are Damaran. A 25-30° local vertical-axis correction was made on our mean paleopole after restoration of folding. This sense of correction on rocks of the Doornpoort Formation also better aligns Damaran overprint poles from the region relative to the polar wander path for the Kalahari Craton. We suggest that rotation most probably occurred during the latest stages of Damaran folding after 500 Ma.

1 Introduction

1.1 Background

The Neoproterozoic supercontinent, Rodinia, existed between ∼900-750 Ma (Z. Li et al., 2008), at a time when the Earth was transitioning between a long period of warm climate to perhaps the most severe ice age it has ever experienced. This study presents new paleomagnetic data for the Kalahari block, which has been proposed to have been near the center of Rodinia (Z.-X. Li et al., 2013). It has also been suggested that differences in the distribution of detrital zircon ages between the Damara-Kalahari and Damara-Congo margins show that these cratons were not together during Rodinia, or if they were in proximity, they may be separated by a rift or oceanic basin (Foster et al., 2015). The movement of the Kalahari and Congo cratons during the assemblage of Rodinia remains largely under debate. Paleomagnetic data for these cratons at 1.1 Ga suggests that they were connected then (Salminen et al., 2018). A younger constraint for their movement and location is given by the onset of the Pan-African Orogeny, a major orogenic system characterized by episodes of collisions related to the assemblage of the Gondwana and Pannotia ca. 600 Ma. The Pan-African and the Grenville orogeny are the largest known orogenic systems throughout Earth's known history. The Damara Orogeny was an episode which occurred due to the collision between the Kalahari and Congo cratons in the early Cambrian. This convergence has been suggested to be 590 Ma, followed by a brief interruption due to the closing of the Adamastor Ocean, with the final collision which formed the Damara Belt occurring 530 Ma (Lehmann et al., 2016).

1.2 Tectonic setting

This study presents new paleomagnetic data for the Rehoboth Basement Inlier of the Kalahari block. This region is immediate to the Pan-African Damara Orogen which was most active between 550-500 Ma (Foster et al., 2015; Goscombe et al., 2018). The Damara Orogeny rose during plate convergence between the Congo and Kalahari Cratons, and widespread parallel fold structures throughout the Rehoboth province have been thought to be due this deformation event.

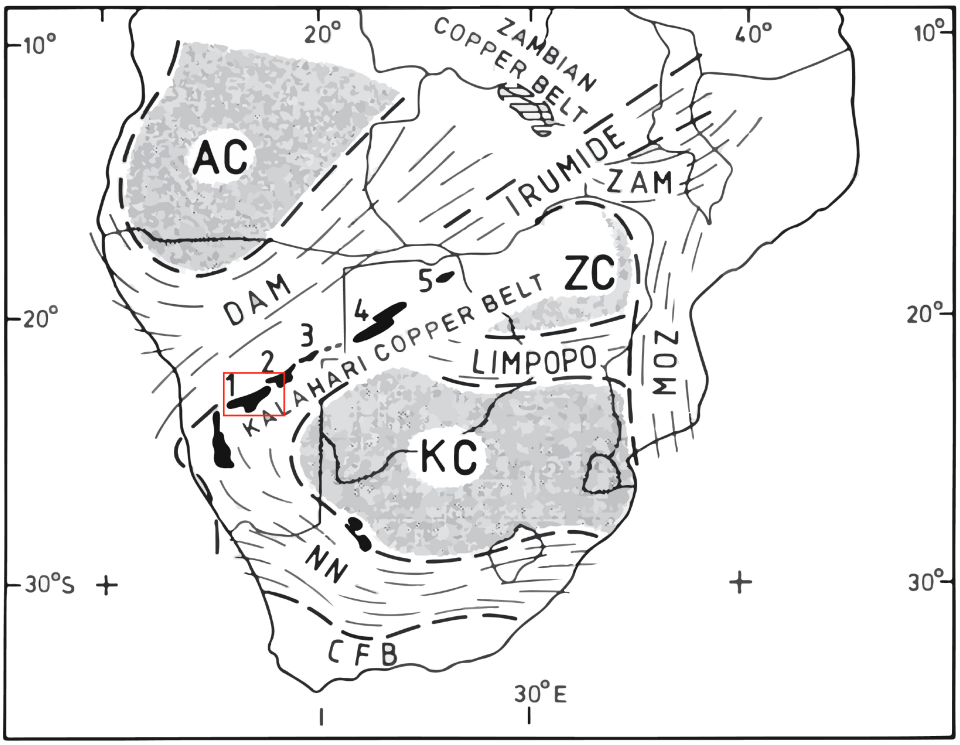

Figure 1: Region of interest (red polygon) in relation to the Kalahari Craton (KC) in present-day Southern Africa. Taken from Borg & Maiden (1989).

Here, we present a paleomagnetic regional survey to explore the spatial and temporal evolution of the RBI during the Meso-Neoproterozoic. The sample suites included in this study encompass the Meso-Neoproterozoic domain of the Rehoboth Inlier.

2 Regional stratigraphy

2.1 Regions of interest

This study includes 12 sample sites, each containing 7-8 rock cores for a total of 84 samples. These samples represent a survey of the younger stratigraphic succession within the Rehoboth region, namely the Klein Aub (C19K), Versailles (V19V), and Tsumis regions (V19T). Overall, these sample suites describe a range of Meso-Neoproterozoic volcanic and sedimentary rocks in the stratigraphic succession of the Rehoboth Inlier. Samples from the Klein Aub region (C19K) are from an unnamed mafic dyke suite, where cross-cutting was observed and baked contact tests are

possible. The Versailles and Tsumis regions (V19V & V19T) include samples from the Doornpoort Formation, described as red-bed sediments (Becker et al., 2005). V19V and V19T were sampled along an anticline and are suitable for a fold test.

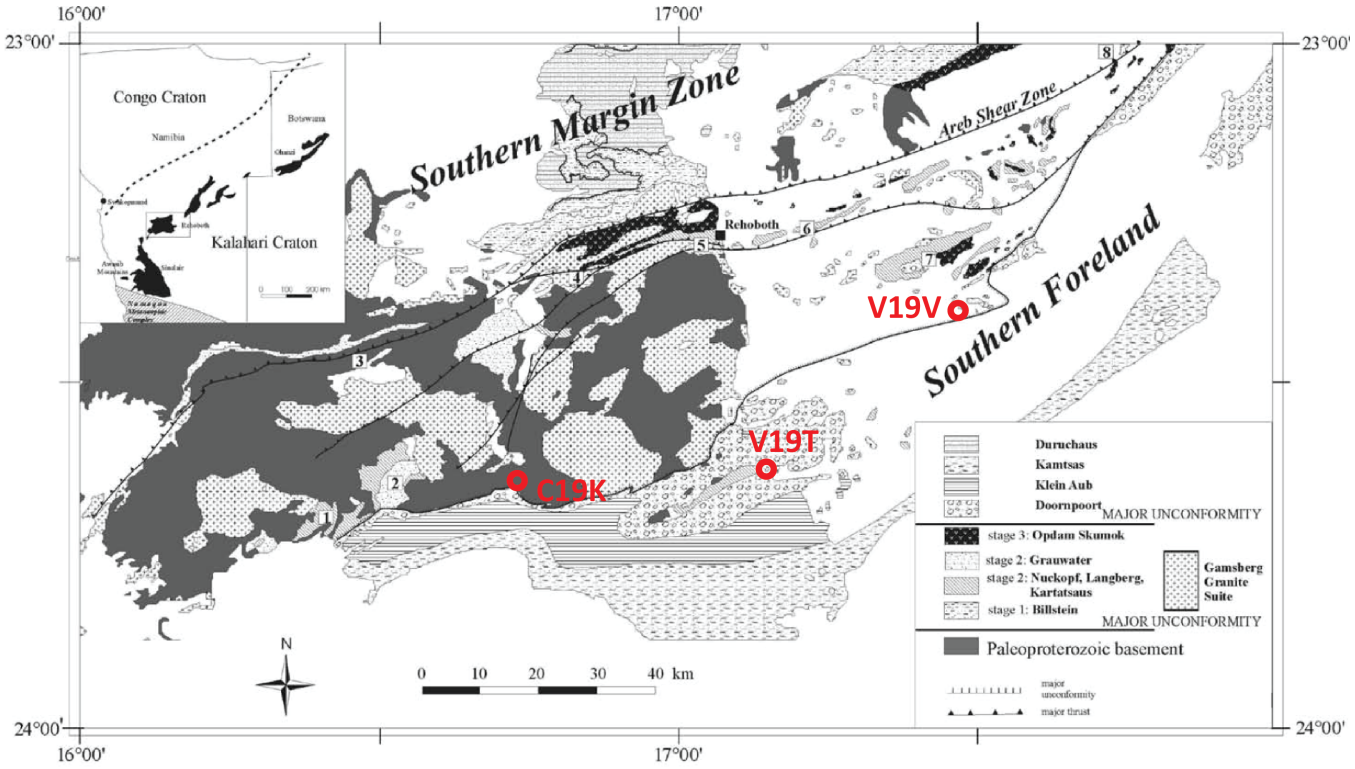

Figure 2: Location of sample suites. Taken after Schneider et al. (2004).

2.2 Age constraints on sample suites

Age constraints for these sample suites are avilable from the country rocks of the Rehoboth Basement Inlier. C19K samples were collected from a cluster of mafic dykes intruding granitic country rock. The different orientations observed for these dykes may suggest that this cluster includes multiple generations of magmatism. The country rock is part of the Palaeoproterozoic Piksteel Granitic Suite, for which the ages are 1781 $\pm$ 8 Ma (van Schijndel et al., 2014). We also consider a minimum age constraint from the sedimentary sequence cover of the Klein Aub region south of where C19K was sampled. The post-sedimentary cover at C19K begins with the Doornpoort Formation, which has been suggested generally as mid-Neoproterozoic, deposited at the start of the Damaran orogenic cycle (Foster?).

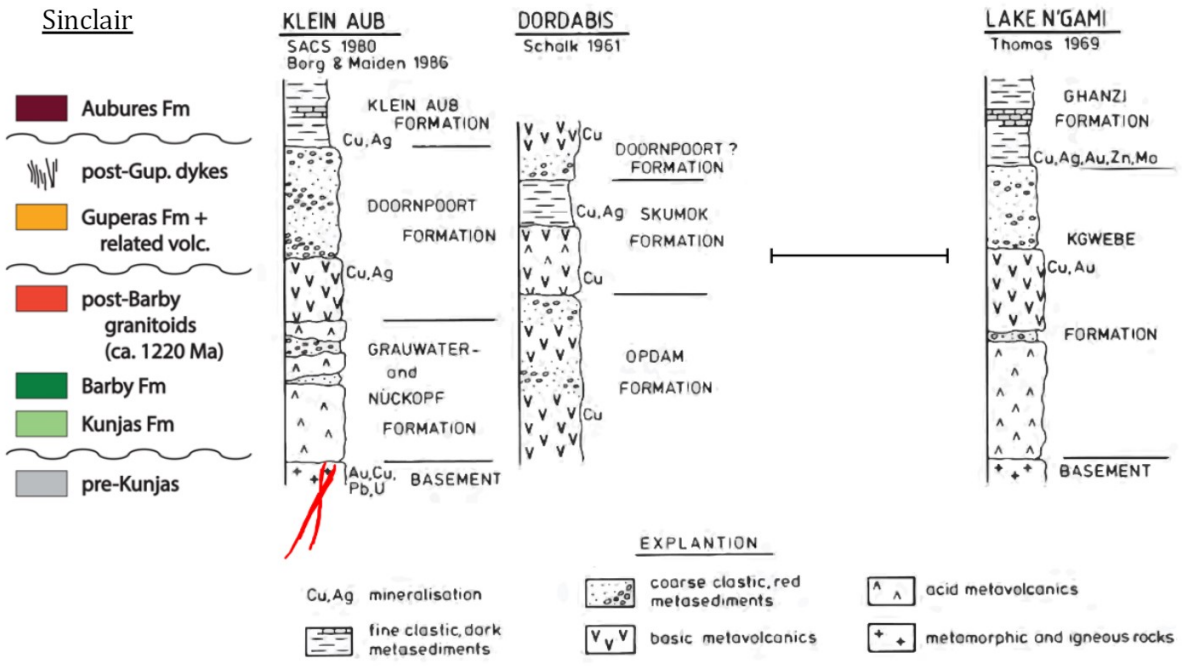

Figure 3: Stratigraphic correlation between the Sinclair, Klein Aub, Dordabis, and Lake N'gami regions. C19K sample suite corresponds to cross-cutting dykes intruding only the basement in the Klein Aub Region, although some may be younger than the Nuckopf Formation, for which the SHRIMP zircon age is 1226 ± 11 Ma (Becker et al., 2005). Figure modified after Borg & Maiden (1989) and (Kasbohm et al., 2016).

The V19T sample suite includes both red-beds and volcanics from the Doornpoort Formation. Samples from T1, T3, and T4 are purple-red sandstones, and samples from T2 are from a massive basaltic lava. The V19V sample suite also includes red-bed sediments from the Doornpoort Formation. Although there is no direct age constraint on the Doornpoort Formation, a possible age constraint can be made from its stratigraphic correlation with a unit of similar composition in the Dordabis region, where the presumed Doornpoort Formation lies above the Opdam Formation (Borg & Maiden, 1989). The Opdam Formation has been observed to overlie the Langberg Formation for which a U-Pb SHRIMP age is 1100 ± 5 Ma (Becker et al., 2005).

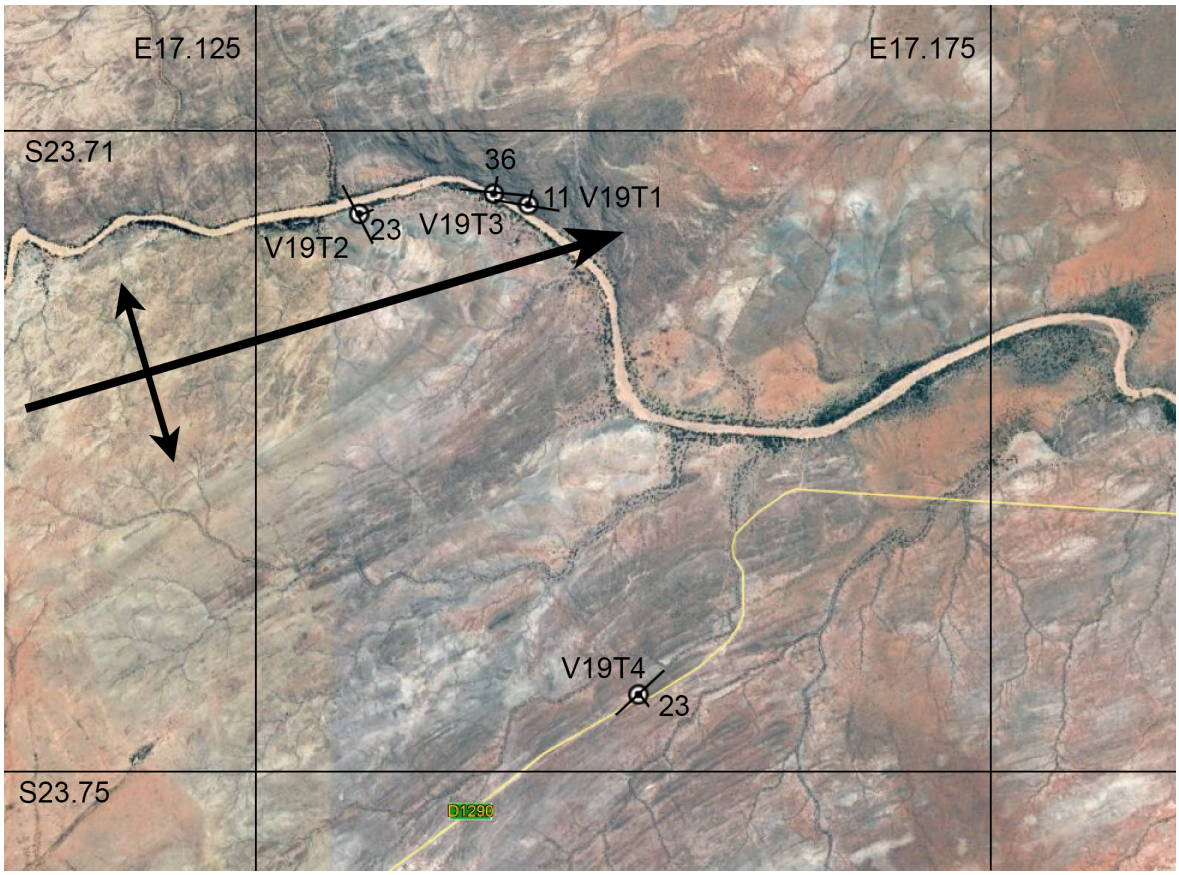

Figure 4: V19T site sample locations and the direction of the anticline from which they were retrieved. Declination and inclination of each sample site are also labeled.

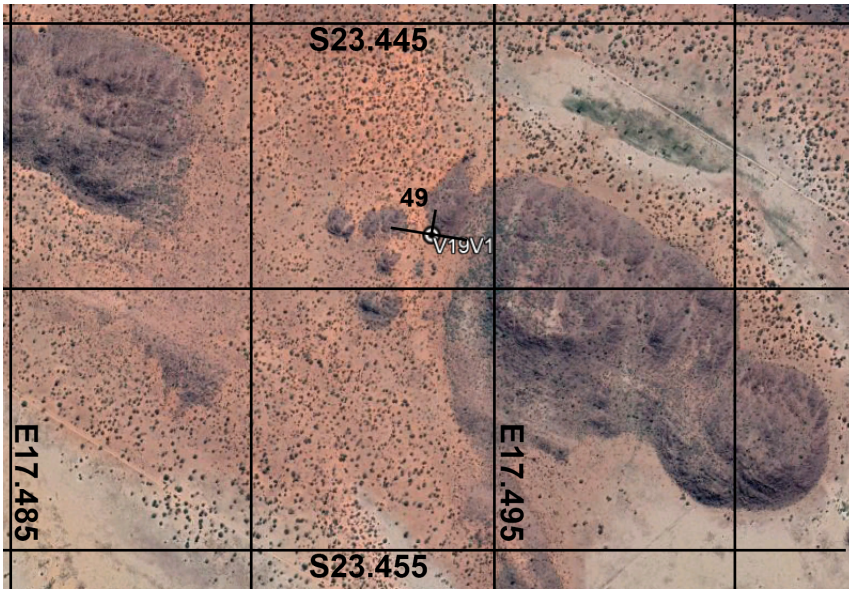

Figure 5: V19V site location.

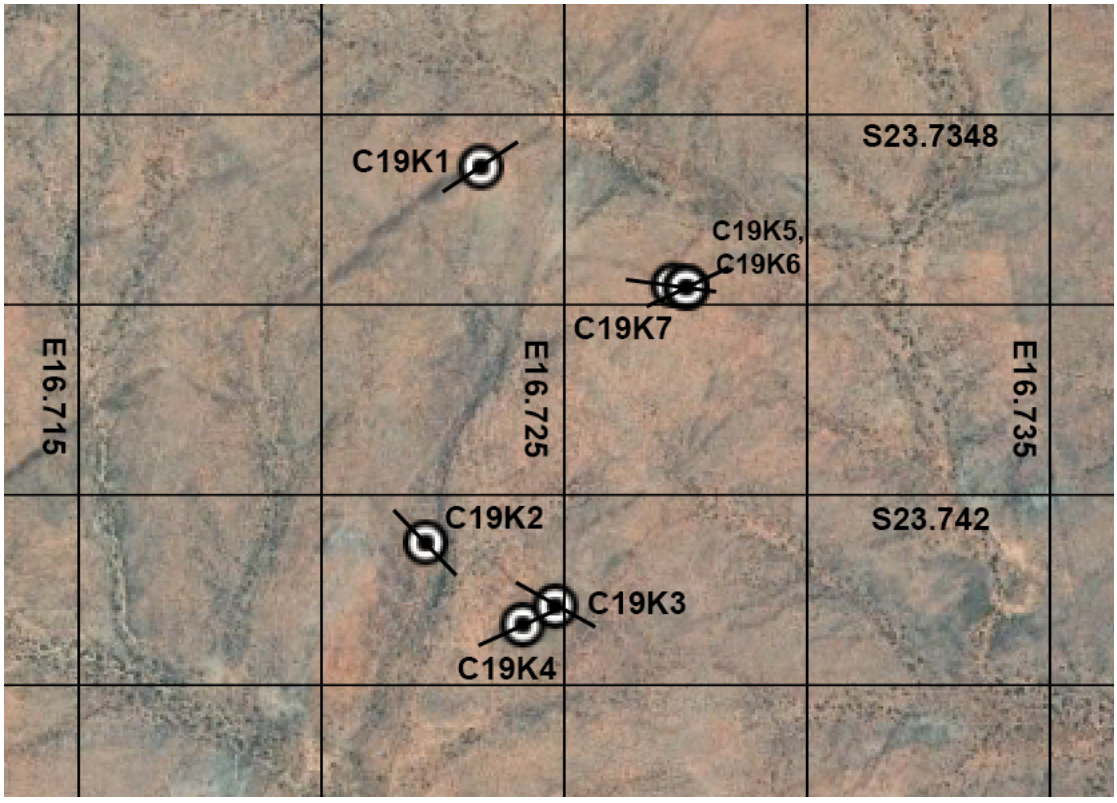

Figure 6: C19K site sample locations with each respective strike shown. Dips were unknown. Sites C19K6 and C19K7 are from the the same location.

3 Methods

3.1 Field

Samples were collected from a number of farms in the Rehoboth region over a three-week expedition in the summer of 2019. Areas of interest were first mapped on Google Earth satellite images with roads, dykes, and farm boundaries identified. Permission for access to these sites were granted by their respective landowners. Specific sites were chosen in the field after surveying the area for potential outcrops. Once identified, outcrops were tested for magnetic susceptibility and compass deflections to minimize chances of sampling from lightning-struck rocks. Typically 7-8 samples are collected from each of these suitable outcrops.

58

Location _____ Date 21 JULY, 2019 (STILL)

BACKTRACK TO NW-DYKE, GREENSTONE w/FELDSPAR PHENOCRYSTS (?)

C19K2 23.74285°S / 016.72226°E / 1539m

- 7±1m wide
- X = 408-577 e-6 SI

LOCAL TREND 330° mag, BUT GOOGLE EARTH SHOWS MORE OF A WNW-TREND.

DIP UNKNOWN (LOW RELIEF, NO COOLING JOINTS)

- COUNTRY ROCK IS ARCHEAN GRANITE
- +1 BIOTITE GEOCHEM/CHRON
- LOTS OF Chlorite and epidote

MONSTER	MAG	HADE	SUN	t	Δ m-s
A	264	20	064	12:44	200
B	235	15	036	12:45	199
C	171	27	332	12:46	199
D	148	16	310	12:48	198
E	110	25	271	12:49	199
F	081	06	244	12:50	197
G	084	11	248	12:51	196
H	006	10	170	12:52	196

59

Location _____ Date _____

Project / Client _____

Scale _____ same porphyritic dyke as K2,

C19K3 but with exocontact of NE striking K4 dyke, which should be younger.

S 23.74404° / E 016.72494° / 1543m

X = 407 - 589 · 10⁻⁶ SI

Str = 135° (OLDER STRIKE) Width = 9±1m

SAMPLE DISTANCES FROM MARGIN OF YOUNGER DYKE

MONSTER	DIST(m)	MAG	HADE	SUN	t	Δ m-s
A	2.70	265	25	107	1509	158
B	2.65	270	22	112	1508	158
C	3.20	264	41	107	1510	157
D	3.10	264	36	109	1513	155
E	3.40	248	40	094	1518	154
F	3.50	285	39	128	1526	157
G	3.35	283	29	129	1521	154
H	3.70	272 (263)	18	110	1523	162/153

- HERE, THE YOUNGER DYKE IS 6±0.5m
- YOUNGER DYKE HAS CHILL ZONE ADJACENT TO COARSE INTERIOR OF THE PORPHYRY, ESTABLISHING THE AGE RELATION, BUT NO VISIBLE CONTACT EXPOSED

Figure 7: Diamond-bit drill used to collect cores (top left) and the holes from which 2.5-cm-diameter cores were collected (top right). Example of notes taken in the field (bottom).

A diamond-bit drill was used to collect cylindrical samples, which are originally ∼5-7 cm in length and ∼2.5 cm in diameter, although fractured samples are often shorter. The inclination, declination, and sun direction for each sample are measured in-situ using an orientation device with solar and magnetic compasses and a clinometer. For sample suites V19V and V19T, the strike and dip of the bedding was measured for use in a fold test. For sample suite C19K, the dip of dykes was not measurable due to low topographic relief. Once removed from the original rock, the direction of drilling are labeled on the sample, with the weathered ends marked.

3.2 Laboratory

Fractured samples are wrapped in laboratory parafilm to hold shape during the preparatory process. At the Yale Kline Geology Laboratory rock lab, samples are first trimmed from the ends using a dual-blade rock saw. All samples are trimmed down to a length suitable for use with Kappabridge magnetic anisotropy systems.

Samples are first measured for magnetic anisotropy (AMS), which is used to identify whether the primary natural remanence magnetization (NRM) was acquired without directional bias. This step is necessary to determine whether magnetic minerals in the samples are randomly oriented such that bias in the alignment of their electronic spin states are minimal, and to check whether this assumption is satisfied. Samples showing strong anisotropy must have their remanence vectors corrected, which will increase the uncertainty of the overall data. While samples showing weak anisotropy do not need to be corrected, they are still useful in helping determine whether the NRM is primary or metamorphic. However, none of the sites were found to be significantly anisotropic, and we will not further discuss AMS measurements.

Figure 8: Prepared and labeled samples ready for demagnetization steps.

All samples are then cut in half and re-labeled. The initial NRM is measured before the demagnetization process. Samples are submerged in liquid nitrogen for > 12 hours as the first step of the degmagnetization process. After this initial step, the magnetic directions are measured using a cryogenic SQuID magnetometer. All subsequent thermal demagnetization steps are done in magnetically shielded ovens which bake samples under increasing temperature steps. The gradual unblocking of the magnetic direction is monitored after each step so as to decide the following magnitude of temperature steps.

Although we expect magnetite and hematite to be the primary magnetic minerals in the samples, with the corresponding Curie temperatures of 580°C and 675°C, respectively, samples are heated for a number of steps beyond these points to ensure that they have fully unblocked. Fully demagnetized samples show a distinct zig-zagging in their magnetic directions as they begin to carry the ~10 nT magnetic field inside the oven, resulting in a zig-zagging behavior as samples are flipped at each step.

Evidence of lightning strikes are monitored for each sample using several diagnostics. The magnetic intensity for lightning-struck samples ($> 10^{-3}$) are typically larger than non-lightning-struck samples ($< 10^{-3}$). Lightning struck samples are also typically single-component if the

samples were fully re-magnetized. Finally, lightning also tends to produce individual samples which appear well-behaved but a mean site magnetization which is poorly clustered.

3.3 Data analysis

Once all samples were fully demagnetized, results are analyzed on PaleoMag software version 3.1b6 (Jones, 2002). Least squares regression was used to fit lines and planes to magnetic components, which are distinguished by eye on on zjiderveld diagrams, where the three-dimensional magnetic directions are projected to north-southand east-west axes. Once identified, components are fitted and labeled. Typically, the high-temperature component of multi-component magnetizations are used as the characteristic remanance direction. For samples where components were too difficult to be distinguished from noise, a plane (HPL) and stable end point (SEP) were used instead. For each site, the characteristic direction for each sample are plotted on a least-squares equal-area plot. Fisher statistics (R. Fisher, 1953) was used to characterize the degree of clustering. If clustering appears to be bimodal or elliptical, a Bingham distribution was used instead. The following sections summarize the least-squares fits for each site.

4 Results

4.1 V19T1

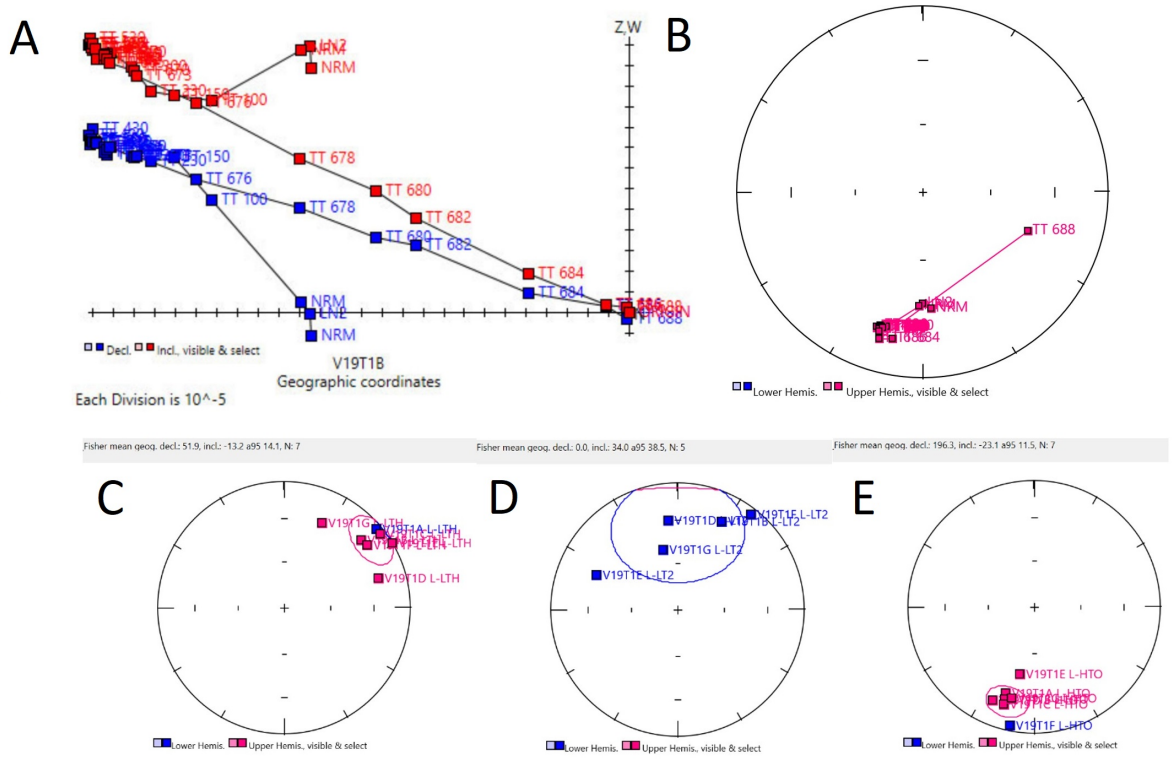

Figure 9: Representative demagnetization behavior from site V19T1. (A) Zijderveld diagram of sample V19T1B, showing three distinguishable components of the NRM. (B) Equal-area stereonet diagram of sample V19T1B. (C) Equal-area plot of the LTH component. (D) Equal-area plot of the LT2 component. (E) Equal-area plot of the HTO component.

The site was in redbeds of the Doornpoort Formation, with a shallow northeasterly dip. Samples contained either two or three well-defined linear components of the NRM. The first to be removed (LTH), either from the NRM or the LN2 step and continuing to typically 100° or 150°C, is directed northeast and shallow. Five samples contained a second low-temperature component (LT2) that was typically removed between about 150° and 430° or 490°C, with an imprecise distribution north and downward. All seven samples had very well-defined decay-to-origin demagnetization held by hematite (HTO) between 670° and 688°C, with a precise cluster of directions SSW and shallow up.

4.2 V19T2

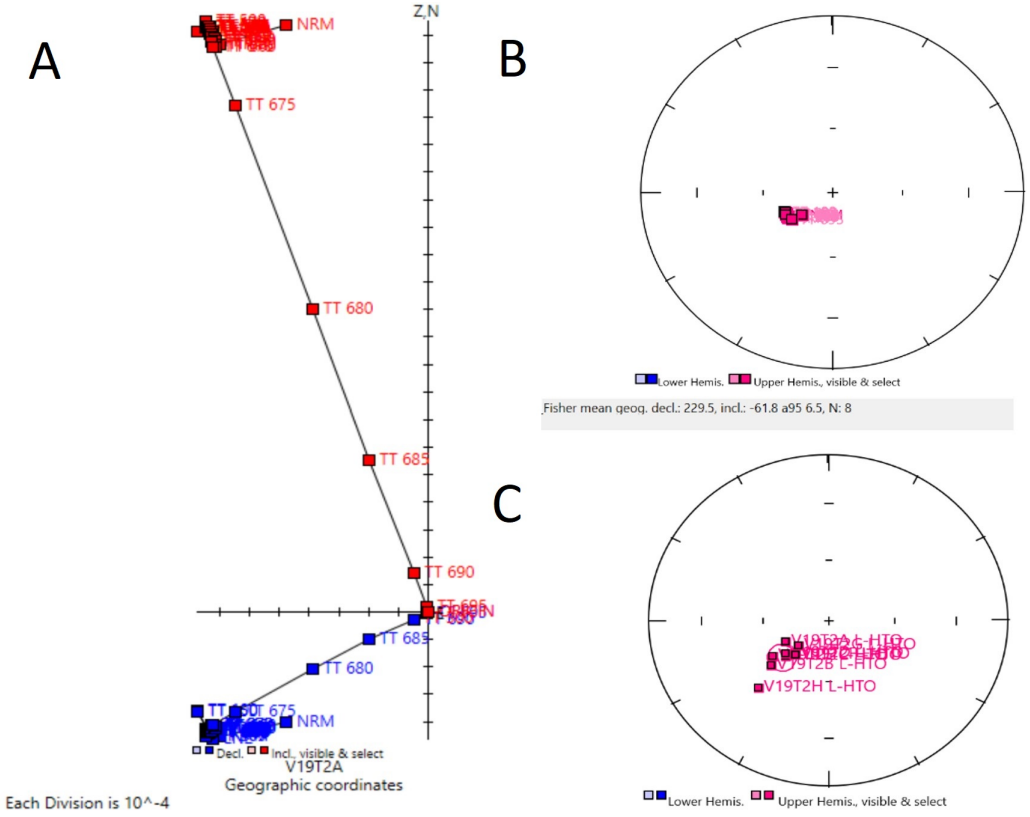

Figure 10: (A) Representative demagnetization path for the sample suite. Many samples had an initial unblocking due to the NRM step; however, since only the NRM step showed this unblocking, this step was not considered to be a component. (B) Equal-area stereonet diagram of sample V19T2A. (C) Equal-area plot of the HTO component.

The site was a massive basaltic lava in the Doornpoort Formation. Samples contained a single-component of the NRM. All eight samples had well-defined (all < 1.4 MAD) decay-to-origin demagnetization held by hematite (HTO) unblocked between 665-670°C, all showing SW and up directions in geograpghic coordinates.

4.3 V19T3

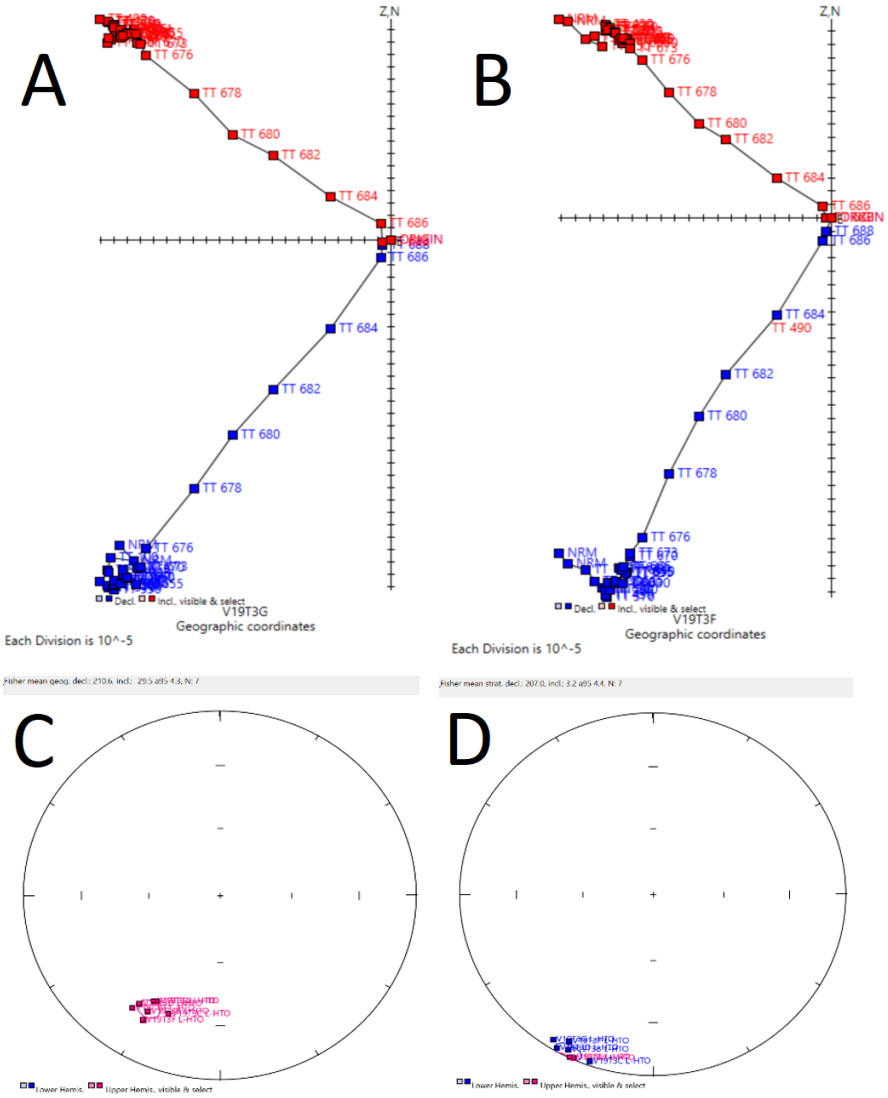

Figure 11: (A) Representative diagrams of single-component and (B) two-component NRMs. HTO components are well-defined and clustered around a shallow SW direction, in geographic (C) and tilt-corrected (D) coordinates.

The site is representative of redbeds of the Doornpoort Formation Of the seven samples, three showed two components and the rest showed a single-component NRM. Of the three, the first low-temperature component (LTH) unblocked either from the LN2 or NRM step and continues to 150°C, with variable directions. Two were in the NE direction and one was in the NW direction. The high temperature components (HTO) unblocked between 665 – 676°C, and all samples showed

a shallow SW direction.

4.4 V19T4

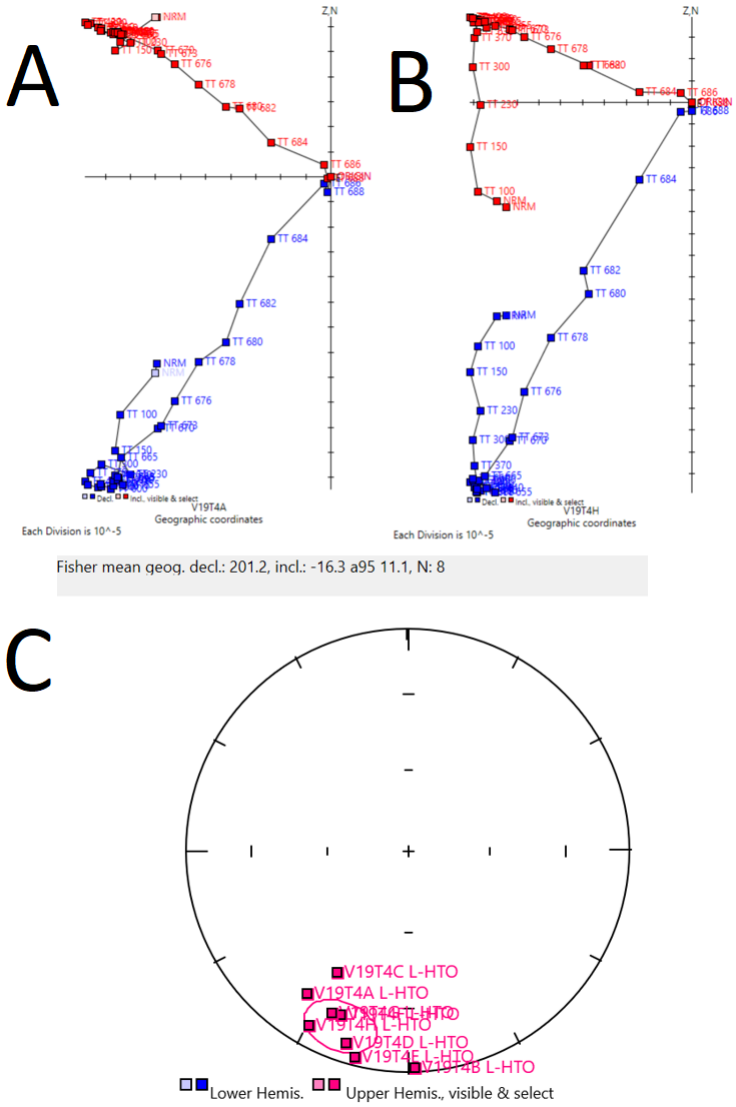

Figure 12: (A) Representative three-component NRM, where the low (LTH) and low-medium temperature (LT2) component appeared to be separate. (B) Representative two-component NRM, where a low to medium temperature component (LMT) was unblocked before the high temperature component (HTO). (C) HTO components in geographic coordinates cluster in the shallow SSW direction.

The site is collected from redbeds from the Doornpoort Formation Of the eight samples, five showed two-components NRMs characterized by a low-medium temperature component followed by a high-temperature component. The first component was unblocked typically at the NRM or LN2 step and continuing until 430°C. One sample had only a low-temperature (LTH) component, running from LN2 to 150°C, followed by a high-temperature component running from 665°C through the origin. The two other samples showed separate components at low and medium temperatures.

4.5 V19V1

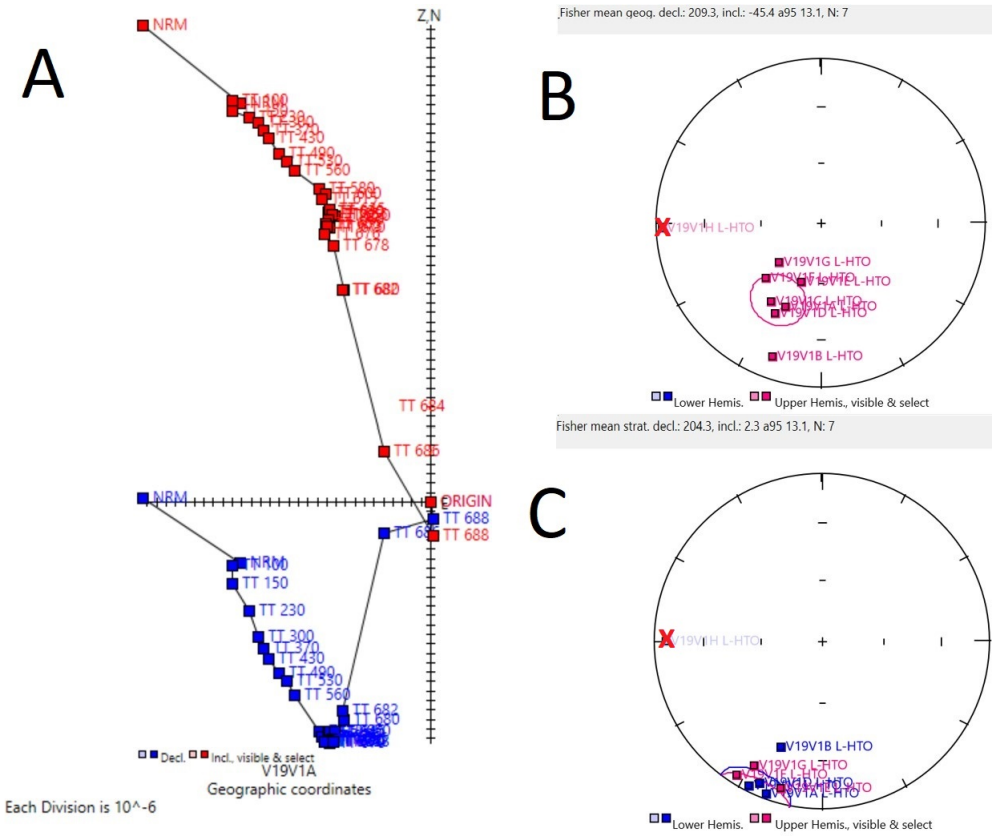

Figure 13: (A) Typical sample showing gradual unblocking from low to medium temperatures. The HTO component was clustered in a SSW-upward direction in geographic coordinates (B) and shallow SSW direction in tilt corrected coordinates (C), with the exception of one sample V19V1H which showed a shallow west direction. This sample has been excluded in the calculation of the Fisher mean.

This site was sampled from redbeds of the Doornpoort Formation. All samples showed a consistent and gradual unblocking between low and medium temperatures for which a low-medium temperature (LMT) component was fitted. This LMT begins and ends at variable temperatures, although most began 230°C and continues to 560°C. Some showed a gradual unblocking throughout the entire demagnetization process, from the NRM step to 600°C, or from 230° to 676°C. The LMT component is scattered across the site, although most directions were south-trending. A high-temperature component held by hematite (HTO) occurred consistently between 676-680°C. Some higher domain components removed by the NRM and LN2 step appeared to be parallel to the HTO-component, suggesting that perhaps some magnetization held by hematite was removed during the LN2 step.

4.6 C19K1

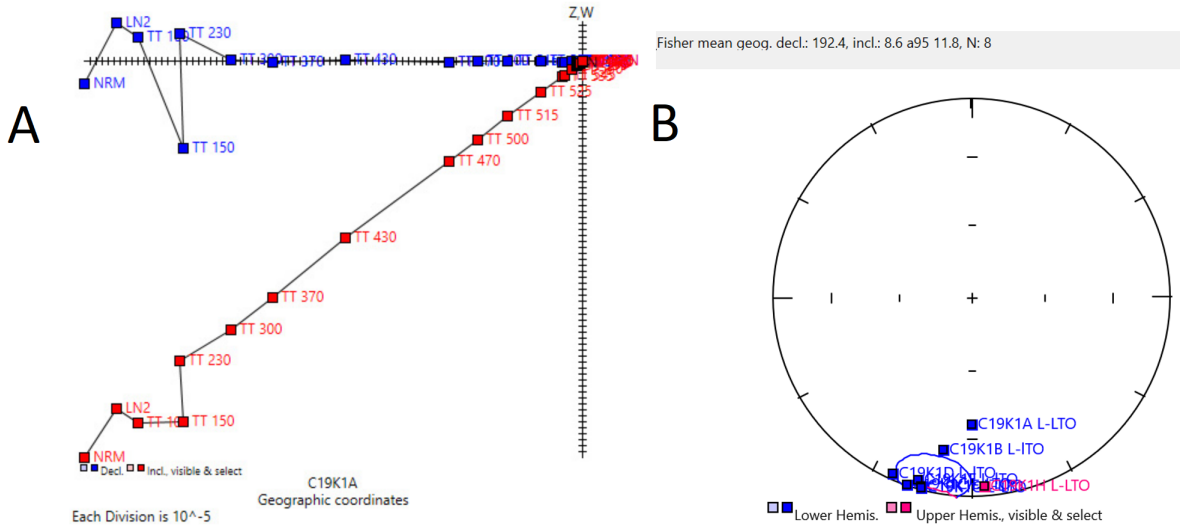

Figure 14: (A) Typical single-component magnetization removed at medium temperatures and continuing into 500°C. (B) All magnetic directions appear clustered in the shallow SSW direction.

This data suite is sampled from a lower greenschist-metamorphosed mafic dyke cutting a granite gneiss basement. All magnetizations were single-component, and no tilt-correction was possible. Overall, the site seems to be clustered in the SSW shallow direction. The removal at middle temperatures beginning at 300°C and continuing into 500°C suggests that a combination of minerals

held this magnetization: magnetite with titanium, Titanohematite, or Titanomaghemite, among other possibilities.

4.7 C19K2

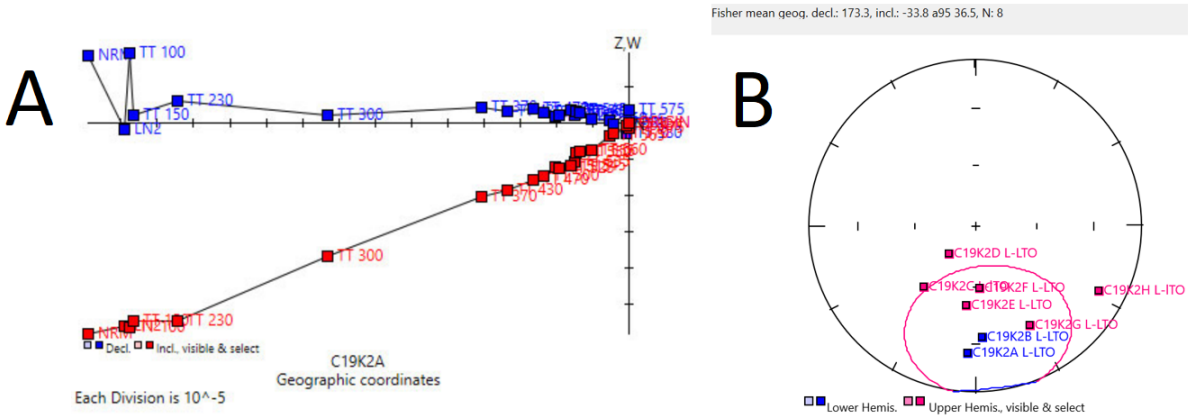

Figure 15: (A) Representative single-component magnetization removed at low temperatures. (B) Equal-area plot of all site samples showing a poorly clustered south-trending direction.

This sample suite was intended to be part of a baked contact test in conjunction with C19K3 and C19K4. Samples were taken from a WNW-trending dyke. The dip was unknown and no tilt correction was made due to lack of topographic relief. All magnetizations showed a single-component starting at 230°C or 300°C, which an overall imprecise cluster around S direction. The magnetization which appeared to be removed at 230°C could be due to the presence of pyrrhotite, however field notes only noted the presence of chlorite and epidote. The mean direction group is generally southward with considerable scatter in inclination, both positive and negative.

4.8 C19K3

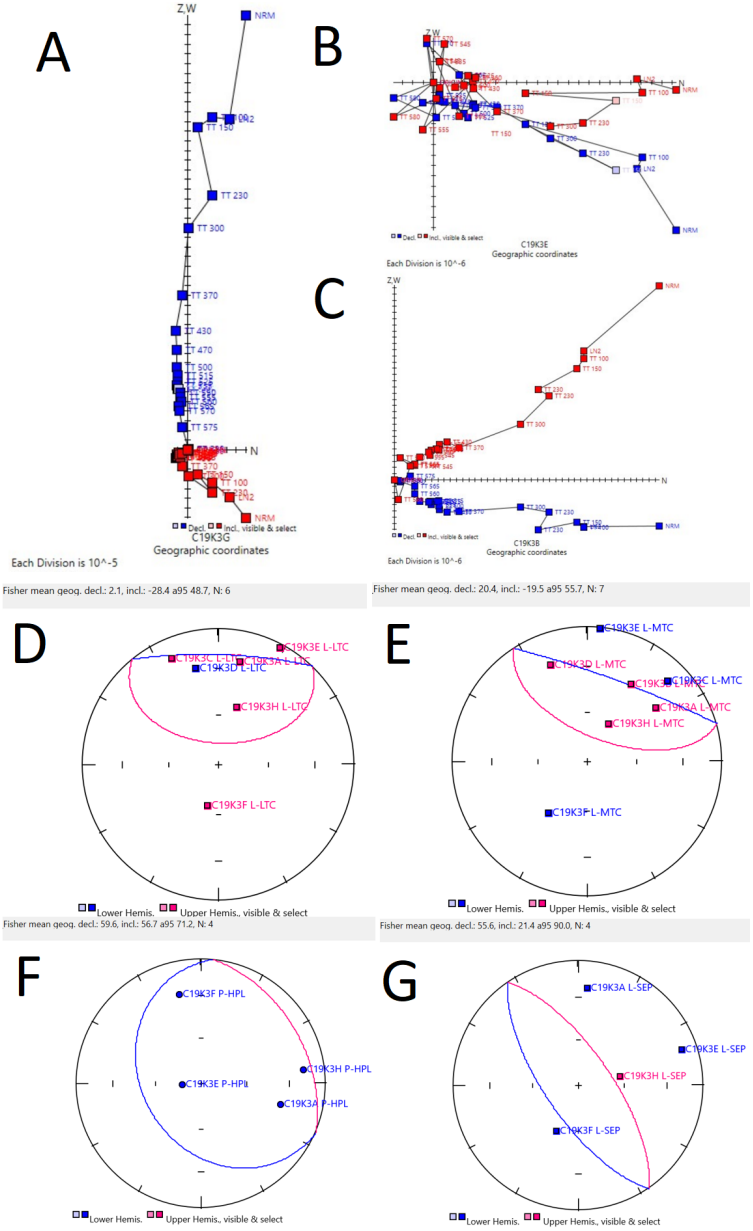

Figure 16: (A) Sample C19K3G showing a single-component magnetization. (B) Representative single-component magnetization showing noisy data around the origin, for which a planar fit (HPL) and stable endpoints (SEP) are used. (C) Representative sample of a two-component magnetization removed at low (LTC) and medium (MTC) temperatures. Equal-area stereonets of the poorly clustered LTC (D), MTC (E), HPL, (F) and SEP (G). All components were too scattered to resolve a typical direction.

This sample suite was collected as part of a baked contact test in conjunction with C19K2 and C19K4. Samples are taken from the same dyke as C19K2, but within the exocontact of the NE-striking C19K4 dyke, which should be younger. Many samples missed the origin but not in a consistent manner, so the noise surrounding the origin was often ignored (530-580°C range) and the fit was instead forced to the origin from the medium temperature component (MTC). For samples with large noise around the origin, a separate planar fit was made. Only one sample showed an apparent one-component magnetization, from 150°C to the origin. The rest were fitted using a low-temperature component (LTC) starting at either 100°C or 150°C and a medium temperature component (MTC) starting and ending at variable temperatures. Four of the samples were fitted using a plane in addition to the MTC, for which the origin was not included. The overall magnetization showed no distinguishable directional clustering.

4.9 C19K4

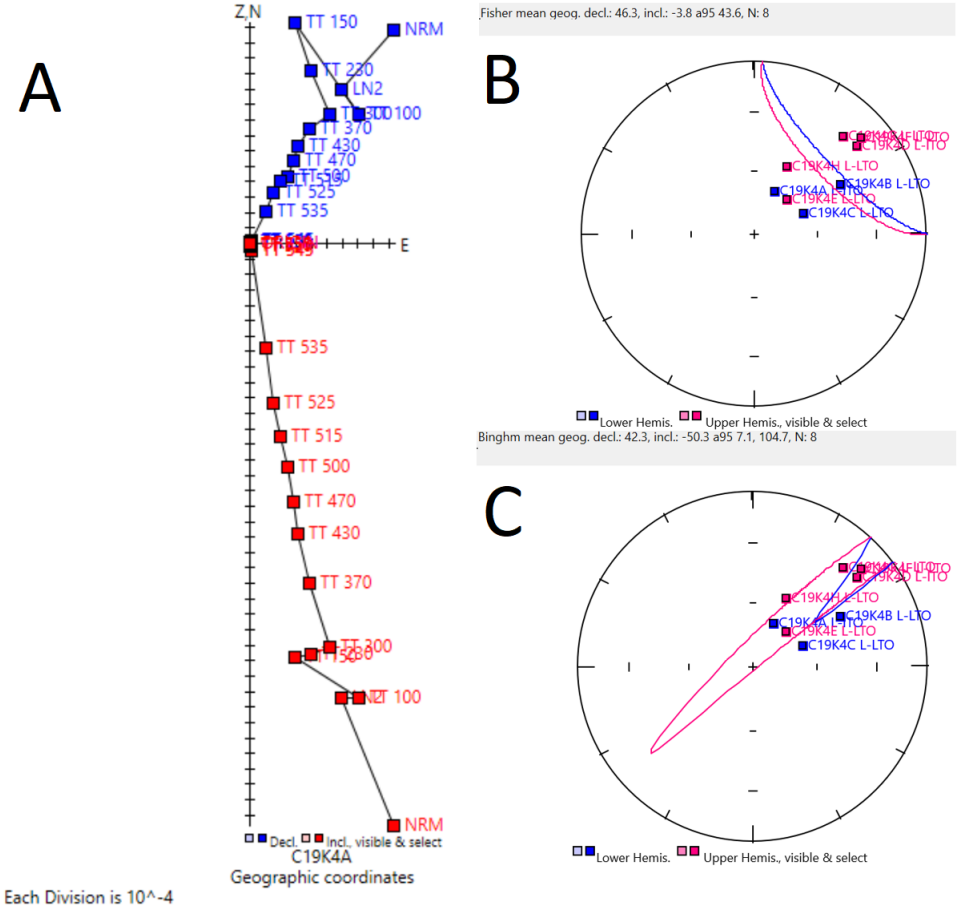

Figure 17: (A) Representative single-component magnetization. (B) A Fisher error with an α-95 value of 43.6, which is above the acceptibility threshold of 20. (C) A Bingham fit which seems to better characterize the distribution.

This sample suite is part of a baked contact test in conjunction with C19K3 and C19K2. Samples are taken from the younger NE-trending dyke of an unknown dip due to low relief. Samples were taken near the southeastern margin of the dyke. All magnetizations showed a single-component, with an imprecise cluster around NE direction. Observing a large spread in the Fisher distribution, the cluster was fitted using a Bingham distribution, streaking between northeast-upward and northeast-downward.

4.10 C19K5

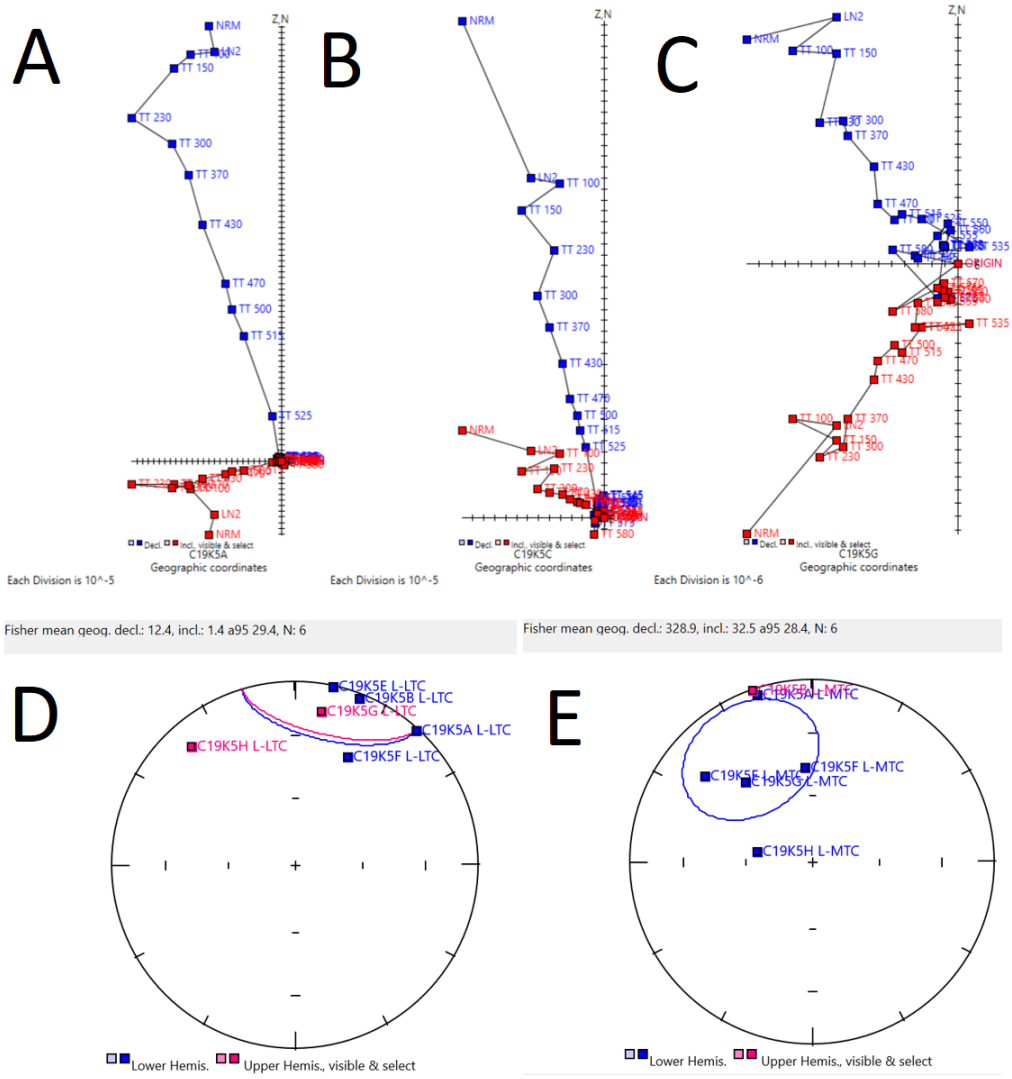

Figure 18: (A) Representative two-component samples. (B) Representative single-component samples. (C) Samples for which a planar fit was used. The LTC (D) showed a typically shallow north direction and the MTC (E) showed a downward NW direction, although neither produced a Fisher mean below the α-95 cut-off.

This sample suite is part of a baked contact test in conjunction with C19K6 and C19K7. Samples are taken from a younger dolerite dyke. Of the eight samples, two showed a single-component magnetization and the rest showed a two-component magnetization composed of a low-temperature component (LTC) beginning and ending at variable temperatures, and a medium-temperature com-

ponent (MTC) beginning at 430°C, 470°C, and 515°C and going to the origin. For samples whose high-temperature domain showed noisy data, a planar fit was made.

4.11 C19K6

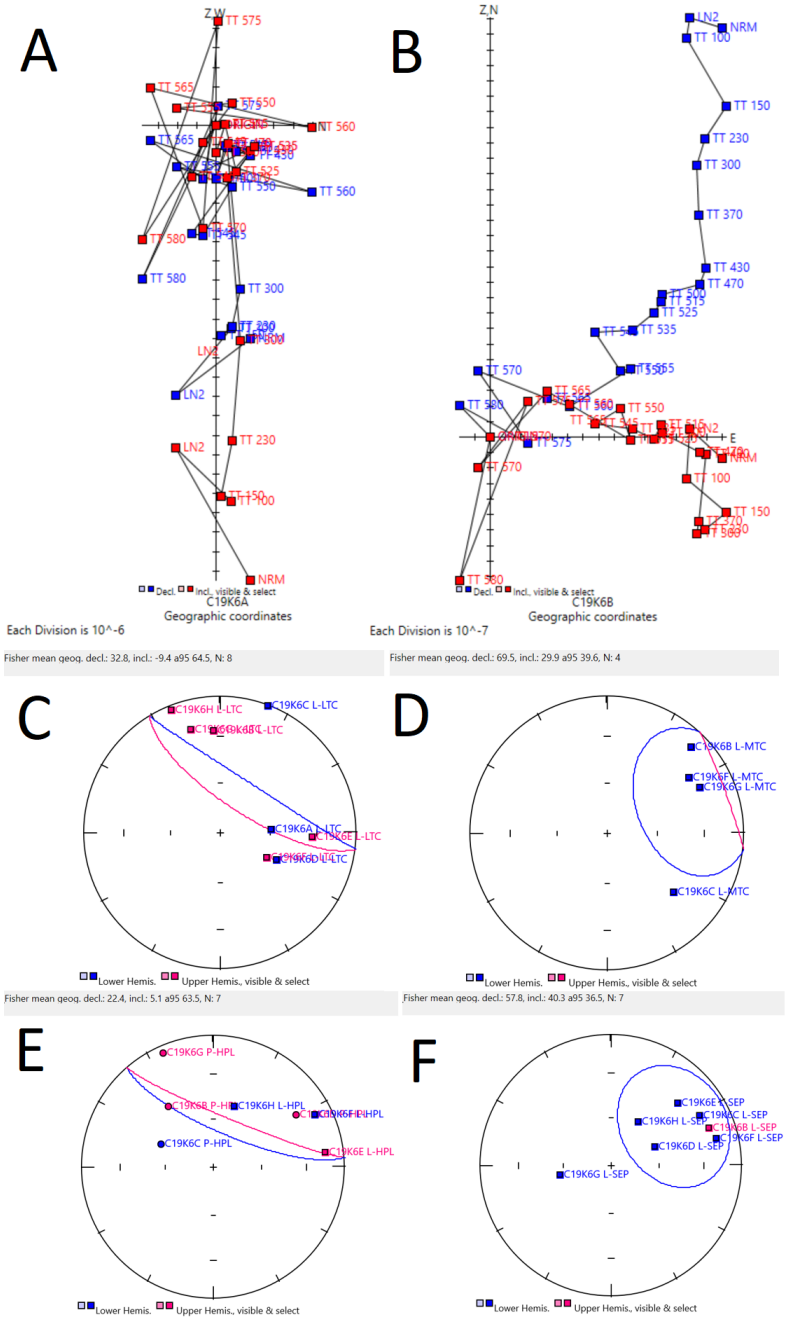

Figure 19: Representative single-component magnetization (A) and two-component magnetization (B). LTC (C) shows a possible NE shallow direction, MTC (D) shows a possible cluster in the NWW direction, HPL (E) shows a north-trending direction, and SEP (F) shows a possible NE trend, although all components are poorly clustered and none meet the α-95 cut-off.

Samples are taken from an older dyke in exocontact of C19K5. After removing noise near the origin, of the eight samples, four showed single-component magnetization and four showed two-component magnetization. Of the two-component samples, there was a low-temperature component (LTC) start at the LN2 step and continuing typically to the 150°C step, except for sample B which appeared to continue to 370°C. The medium-temperature component (MTC) began and ended at variable temperatures. Data points beyond this temperature were too scattered to perform a fit. For the MTCs, a plane was also fitted to include the origin. For single-component magnetizations which appeared to miss the origin due to scattering around the origin, a plane was also fitted.

4.12 C19K7

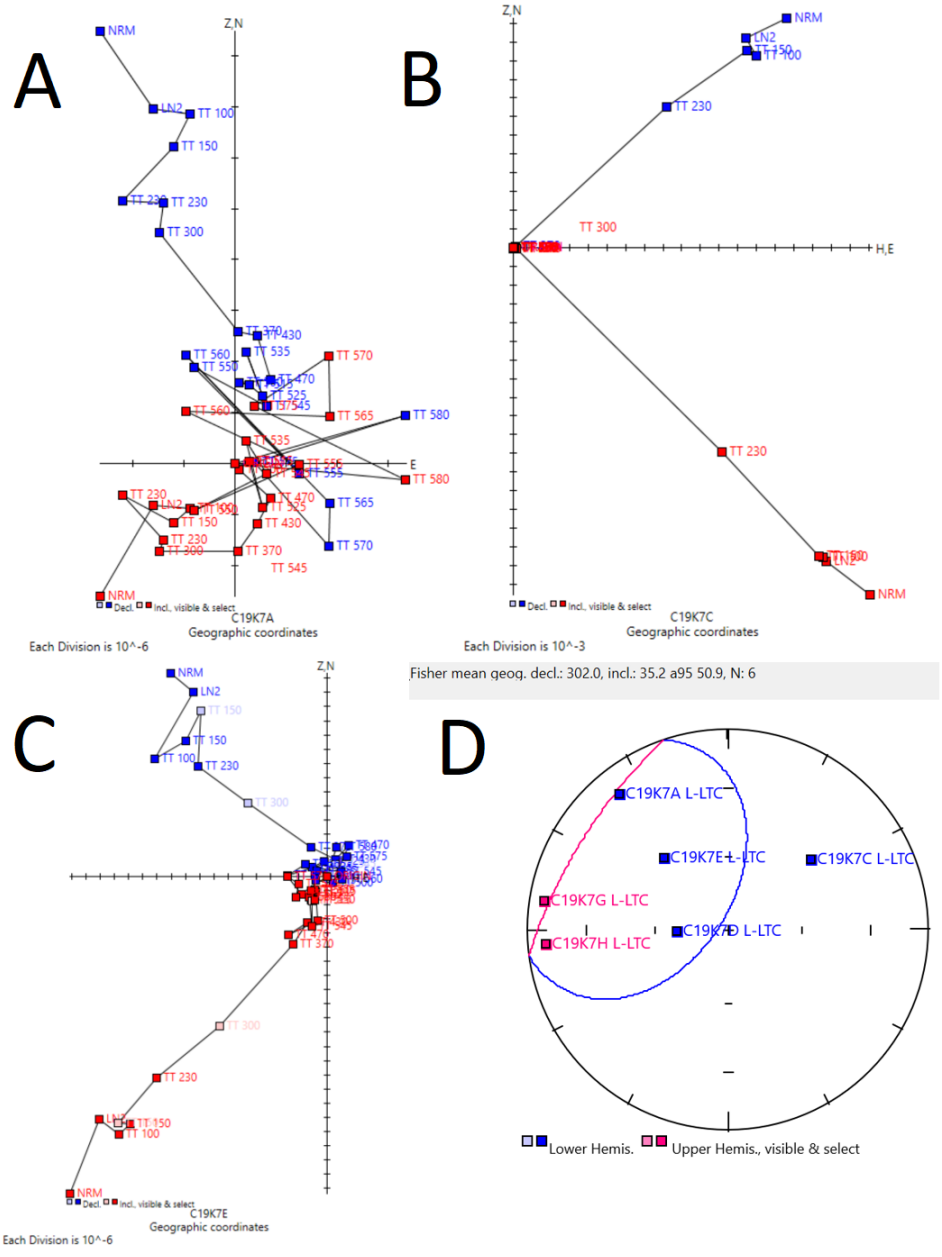

Figure 20: (A) Sample C19K7A showing possibly two components with noise surrounding the origin. (B) Representative single-component magnetization going to origin. (C) Representative single-component magnetization with noisy data at high temperatures. (D) Fisher mean calculated for the single-component magnetizations (LTC).

6 samples were taken from the same dyke as C19K6 at ∼13 m from the dyke in C19K5. All but one sample showed a one-component magnetization going to origin. Sample A had large noise near the origin, and the apparent component seems to miss the origin, so a plane was fitted in addition. A low-temperature (LTC) component and a planar fit (HPL) with a stable end point (SEP) was fitted for this sample. All other samples showed a single-component magnetization, either going to the origin or showing noise around the origin, but appearing to be leading up to the origin.

5 Discussion

Here we interpret our results for the fold test conducted on V19V and V19T. Baked contact tests for the C19K sample suite were inconclusive due to its poorly clustered magnetization. However, we were able to constrain a virtual geomagnetic pole (VGP) from C19K1 and compare it to existing poles for the Kalahari block, although the age of this pole is not yet determined.

5.1 Fold test

The V19T and V19V sample suites provide a fold test for the determination of the timing of their primary magnetization. Typically, if the magnetization was acquired prior to folding, NRM directions should converge at 100% tilt correction, or full restoration of the bedding. Therefore, we expect maximum clustering of points when samples are fully corrected. The amount of clustering is characterized by Fisher's k-value, which is larger for more well-defined clusters and smaller for less defined clusters. The in-situ declination and inclination were used to calculate partial unfolding mean declination and inclination, going from 0 to 100% unfolding. A k-value was calculated for each partial unfolding step, and a maximum value of 24.5 was observed at 60% unfolding. As a check that no single site weighed heavily in the determination of our results, we removed each site's weight in the calculation and found that results remain largely the same. For a sample size of 5 sites, the proportionality between the maximum and minimum k-values needed for results to be statistically significant (with a p-value of 0.05) is 4.43 (N. I. Fisher et al., 1987). However, we find that our proportionality between 0% and 60% unfolding is 1.76, and our results were therefore not shown to be statistically significant. The anticline from which we sampled showed a plunge angle of only ∼10 degrees, and thus the corresponding plunge corrections are

insignificant.

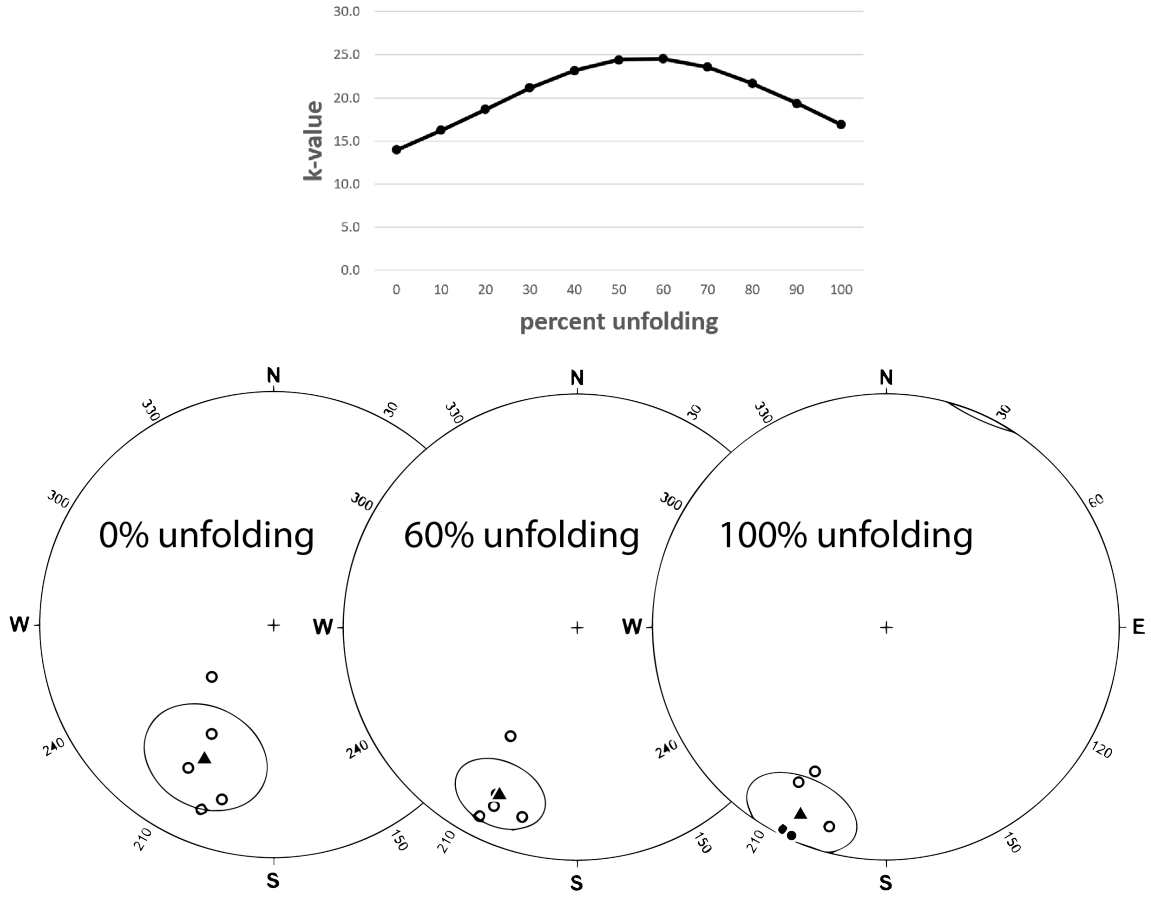

Figure 21: Results of the fold test on V19V and V19T, with the peak in k-value at 60% unfolding shown in inset.

Although our data failed to reject the null hypothesis, we note that the sensitivity of fold tests to the declination suggests that our results are still robust. The apparent peak at 60% unfolding is highly suggestive of a syn-folding magnetization such that NRMs were acquired at the time of folding. Similar syn-folding results were also observed in samples from the Aubures Formation in Kasbohm et al. (2016). The Tsumis Group, which includes the Doornpoort Formation, in the Rebohoth area is thought to be stratigraphically correlated to the Aubures Formation in the Konkiep Subprovince of the Sinclair area (Becker & Schalk, 2008), although direct connectivity of exposure is lacking. We attribute the apparent syn-folding magnetization throughout the Rehoboth Inlier to be representative of a single folding episode.

We suggest a few possible age constraints on the time of folding. Folding must be younger than

the youngest folded rock. Though there are no existing ages on the sampled rocks, we propose a few constraints from the surrounding stratigraphy. The country rock in the Rehoboth Inlier is part of the Piksteel Granitic Suite, for which the TIMS age is 1781 $\pm$ 8 Ma (van Schijndel et al., 2014). Secondly, the Doornpoort Formation lies stratigraphically above the Nuckopf Formation. If this formation is 1226 $\pm$ 11 Ma in age (Becker et al., 2005), then Doornpoort must be younger than this unit. Thirdly, in the region east of Rehoboth, we find the Langberg Formation in sequence with the Opdam Formation (Borg & Maiden, 1989). The U-Pb age for this unit from Becker & Schalk (2008) is 1100 +/- 5 Ma. We suggest that the time of magnetization and therefore folding is probably slightly younger than 1100 +/- 5 Ma.

In the current literature, the Doornpoort Formation is thought to be part of an overall sequence representative of a single tectonic cycle at the time of Rodinia breakup, around 800 Ma (Foster et al., 2015). This is coincident with Rb-Sr ages of dykes in the surrounding region, which is 821 Ma (Ziegler & Stoessel, 1990). However, our results for the magnetization and deformation of the Doornpoort Formation are more consistent with ca. 1100 Ma. If magnetization is indeed ca. 1100 Ma and syn-fold, then not all late-tectonic magmatism in the Rehoboth Inlier is mid-Neoproterozoic. Furthermore, our results are suggestive of an episode of deformation that is Mesoproterozoic in age, and that not all fold structures observed in the Doornpoort Formation are Damaran.

5.2 Poles

Here we present the mean virtual geomagnetic pole (VGP) calculated from sample suites V19V and V19T at 60% partial unfolding. For V19V and V19T, the mean pole direction is 46.9°N, 54.2°E, with an A95 value of 9.4°. Of our 7 sites in C19K, only one gave a good direction, and this direction is the same as those previous reported in other studies. For C19K1, the mean VGP direction is 67.23°N, 50.3°E with an A95 value of 8.5°. Due to an unknown dip on this sample suite, we cannot resolve whether it could have been rotated. Although our pole was constructed only from one dyke, we believe it to have held primary magnetization due to the observed narrow thermal unblocking spectrum near the Curie temperature of magnetite, which is characteristic of mafic dykes with primary remanence.

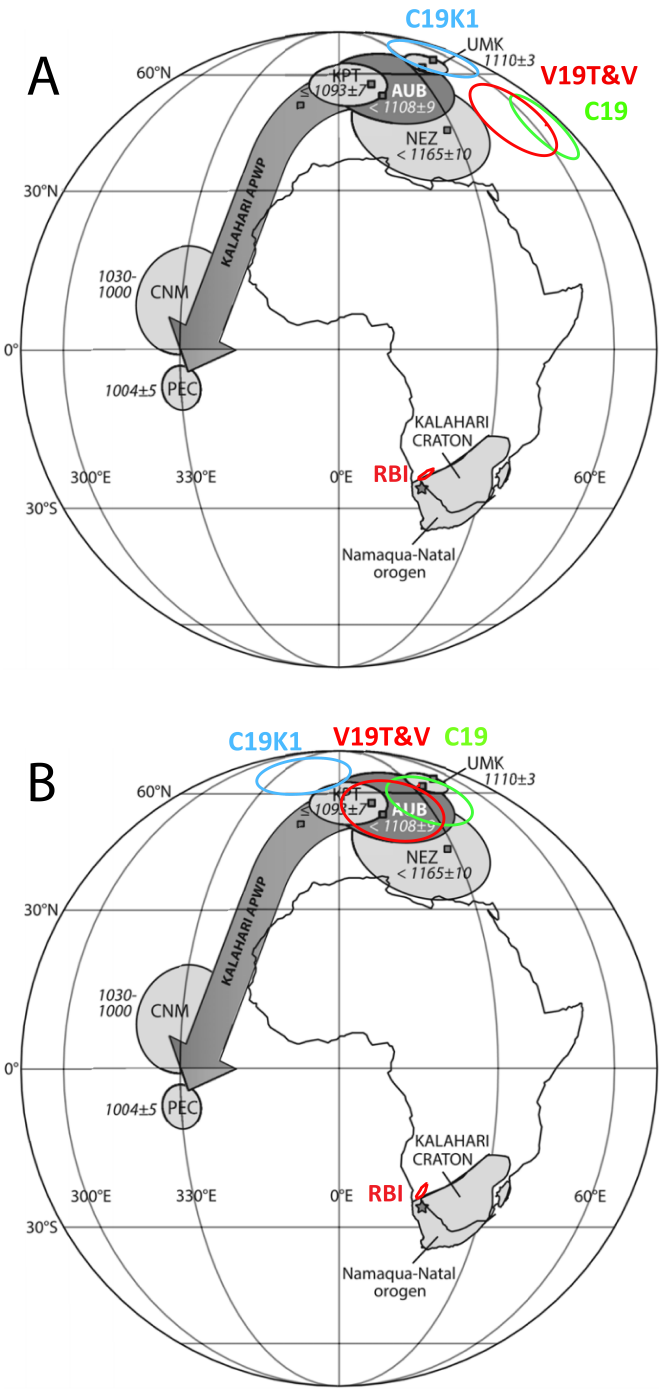

Figure 22: The location of poles calculated from this study's fold test (red), the single site C19K (blue), and the mean of sample suites from Chung-Halpern (2021) (green) are visualized in GPlates software version 2.2.0 (Müller et al., 2018). (A) The original poles. (B) The poles after a 25° Euler rotation about an axis at 24°S, 16°E at the southwestern edge of the RBI. Figure modified after Kasbohm et al. (2016).

The pole direction at 60% unfolding in this study is not consistent with the expected pole directions for the Kalahari Craton between 1200 and 1000 Ma, including that obtained from the possibly correlative Aubures Formation in Kasbohm et al. (2016) (Fig. 22). A 25° counter-clockwise rotational correction appears to restore this pole to the expected apparent polar wander path (APW) for the Kalahari Craton. By rough estimation, we find that a 25° rotation provided the best fit to the expected apparent polar wander (APW) path for the Kalahari Craton (Kasbohm et al., 2016). The suggestive age of ca. 1100 Ma was derived from the corrected pole being more similar to the 1110 Ma Umkondo (UMK) pole (Hanson et al., 2006) but distinct from the 1030-1000 Ma Central Namaqua belt (CNM) pole. Although this provides only an upper age constraint and magnetization could still be Damaran in age, there is no amount of rotational correction that can correct our anomalous pole to the APW path for Gondwana at 550-500 Ma due to our observed shallow inclination. Therefore, we find it most consistent for the age of folding and magnetization to be much closer to ca. 1100 Ma.

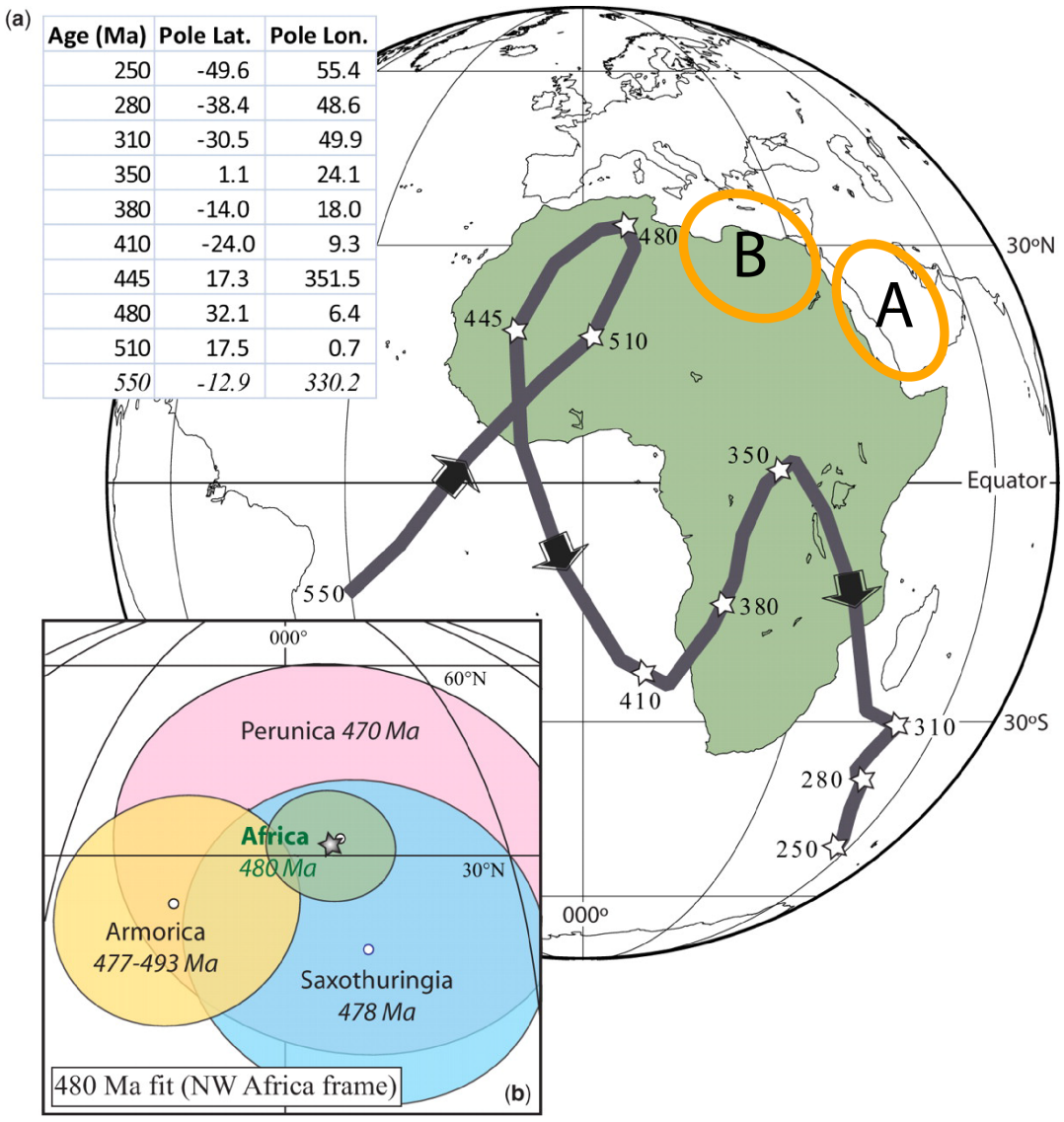

Figure 23: Pole from Piper (1975) plotted before (A) and after (B) a 25° CCW vertical-axis rotation. The APW path for Gondwana at 550-510 Ma (Torsvik & Van der Voo, 2002) is shown for reference. We find that a 25° correction brings Piper's pole to within error of the expected APW path. Figure modified after Torsvik & Cocks (2011).

Piper (1975) also conducted a fold test for rocks of the Doornpoort Formation. He found a post-folding result and interpreted the folding to be of Damaran in age, although we now have suggested that there could have possibly been a much older episode of folding. However, Piper's pole has an inclination which is too steep to be corrected to the APW for South Africa at ca. 1100 Ma. Therefore, following Piper's interpretation, we believe this pole to be an overprint of Damaran

age (550-500 Ma) to suggest a possible time constraint for rotation. Piper (1975) found a pole that did not match any part of the African APW from 1300 to 600 Ma, and for which a 25° vertical-axis CCW rotation correction would place it within error of the expected APW at ∼500 Ma. We attribute the apparent regional correction observed in this study and Piper (1975) to the existence of a microplate within the Rehoboth Inlier having rotated 25° counter-clockwise. Since the pole from Piper (1975) is Cambrian in age, we suggest that rotation occurred after 500 Ma. After Cambrian time, the Rehoboth Inlier would have already embedded itself in Gondwanaland and the mechanisms for rotation would have been limited. The most likely time to rotate is therefore during the latest stages of Damaran folding.

An alternative explanation for this apparent rotation is a more complex structure involving transform faults inside this microplate. This microplate could have been comprised of internal parallel blocks which could individually rotate. Although we have not recognized strike-slip faults in the Rehoboth Inlier, these structures could be subtle or yet recognized.

6 Conclusion

A suspected syn-folding result from our fold test and anomalous poles that appear to be restored to the Kalahari APW path at ca. 1100 Ma after a 25° correction are suggestive of a tectonic evolution more complicated than previously thought for the Rehoboth Inlier. Our results suggest that a deformation event much older than the Damara Orogen could have been active during the Meso-Neoproterozoic. Furthermore, rotation within the region is suggestive of a microplate possibly rotating around 500 Ma, near the end of Damaran folding when a rotational event would have been most probable. We suggest this to be the simplest explanation for the syn-folding magnetization observed throughout three distinct studies (this study; Kasbohm et al., 2016; Chung-Halpern, 2021) on rocks of the Rehoboth Inlier and Konkiep Terrane, as well as the anomalous poles found in this study and Piper (1975). However, we emphasize that the modest sample size does not yet lend itself to a robust interpretation. Here we present a non-unique solution to a problem of limited constraints. Therefore, this study can be bolstered by a larger data set ideally comprised of samples collected in regions where good data have already been observed. This would help better constrain the geographic extent of this rotation in rocks of the RBI, the degree and age of rotation, and test the

reproducibility of our results. Furthermore, the ages of the sampled dykes remain unknown, and we cannot be certain as to which episode of magmatism they represent. Geochronological dating can be used to age dykes in this region, which would allow us to better interpret the pole derived from C19K and dykes of the same generations. Bedding could also be measured for dykes to check whether they may be yielding anomalous poles amenable to vertical-axis rotational corrections.

Acknowledgments

This research was made possible by the Yale College Dean's Research Fellowship which funded the field work in the summer of 2019 and the Karen Von Damm '77 Research Fellowship which funded both laboratory and field work throughout Spring 2019 to Fall 2021.

I extend my sincerest gratitude to my adviser, David Evans, for providing not only academic but personal support, wisdom, and guidance. I thank Richard Hanson of Texas Christian University for offering his time and advice as the second reader. I thank the farmers and landowners who have graciously welcomed us into their land: the Traut family at Gravenstein Farm; the Descande family at Eindpaal Farm; Errico Van Wyk at Naris Farm. I also thank Anna Nguno at the Geological Survey of Namibia for official endorsement of our sampling; Charlie Hoffmann for perennial insights; Johanna Salminen, Ben Mapani and Martin Klausen for field companionship.

Finally, I would like to acknowledge my labmates without whom laboratory work would have been terribly lonely: Chiara Chung-Halpern, Zheng Gong, and a massive thank-you to Jikai Ding, who assiduously demagnetized and measured much of the data presented in this study during the height of a pandemic.

References

Becker, T., Garoeb, H., Ledru, P., & Milesi, J.-P. (2005, 12). The mesoproterozoic event within the rehoboth basement inlier of namibia: review and new aspects of stratigraphy, geochemistry, structure and plate tectonic setting. *South African Journal of Geology*, *108*, 465-492. doi: 10.2113/108.4.465

Becker, T., & Schalk, K. (2008). The sinclair supergroup of the rehoboth volcanic arc from the sossusvlei-gamsberg area to the gobabis region. in: Miller rmcg (ed) the geology of namibia. geological survey of windheok.

Borg, G., & Maiden, K. (1989, 01). The middle proterozoic kalahari copperbelt of namibia and botswana. *Geological Association of Canada Special Paper*, *36*, 525-540.

Chung-Halpern, C. (2021, 05). Reconnaissance paleomagnetism of the northern rehoboth basement inlier, namibia.

Fisher, N. I., Lewis, T., & Embleton, B. J. J. (1987, 08). Statistical analysis of spherical data. doi: 10.1017/cbo9780511623059

Fisher, R. (1953, 05). Dispersion on a sphere. *Proceedings of the Royal Society A: Mathematical, Physical and Engineering Sciences*, *217*, 295-305. doi: 10.1098/rspa.1953.0064

Foster, D. A., Goscombe, B. D., Newstead, B., Mapani, B., Mueller, P. A., Gregory, L. C., & Muvangua, E. (2015, 08). U–pb age and lu–hf isotopic data of detrital zircons from the neoproterozoic damara sequence: Implications for congo and kalahari before gondwana. *Gondwana Research*, *28*, 179-190. doi: 10.1016/j.gr.2014.04.011

Goscombe, B., Foster, D. A., Gray, D., & Wade, B. (2018). The evolution of the damara orogenic system: A record of west gondwana assembly and crustal response. *Regional Geology Reviews*, 303-352. doi: 10.1007/978-3-319-68920-$3_1$2

Hanson, R., Harmer, R., Blenkinsop, T., Bullen, D., Dalziel, I., Gose, W., ... Ward, S. (2006, 09). Mesoproterozoic intraplate magmatism in the kalahari craton: A review. *Journal of African Earth Sciences*, *46*, 141-167. doi: 10.1016/j.jafrearsci.2006.01.016

Jones, C. H. (2002, 12). User-driven integrated software lives: “paleomag” paleomagnetics analysis on the macintosh. *Computers Geosciences*, *28*, 1145-1151. doi: 10.1016/s0098-3004(02)00032-8

Kasbohm, J., Evans, D. A. D., Panzik, J. E., Hofmann, M., & Linnemann, U. (2016, 01). Palaeomagnetic and geochronological data from late mesoproterozoic redbed sedimentary rocks on the western margin of kalahari craton. *Geological Society, London, Special Publications*, *424*, 145-165. doi: 10.1144/sp424.4

Lehmann, J., Saalmann, K., Naydenov, K. V., Milani, L., Belyanin, G. A., Zwingmann, H., ... Kinnaird, J. A. (2016, 01). Structural and geochronological constraints on the pan-african tectonic evolution of the northern damara belt, namibia. *Tectonics*, *35*, 103-135. doi: 10.1002/2015tc003899

Li, Z., Bogdanova, S., Collins, A., Davidson, A., De Waele, B., Ernst, R., ... Vernikovsky, V. (2008, 01). Assembly, configuration, and break-up history of rodinia: A synthesis. *Precambrian Research*, *160*, 179-210. doi: 10.1016/j.precamres.2007.04.021

Li, Z.-X., Evans, D. A., & Halverson, G. P. (2013, 08). Neoproterozoic glaciations in a revised global palaeogeography from the breakup of rodinia to the assembly of gondwanaland. *Sedimentary Geology*, *294*, 219-232. doi: 10.1016/j.sedgeo.2013.05.016

Müller, R. D., Cannon, J., Qin, X., Watson, R. J., Gurnis, M., Williams, S., ... Zahirovic, S. (2018, 07). Gplates: Building a virtual earth through deep time. *Geochemistry, Geophysics, Geosystems*, *19*, 2243-2261. doi: 10.1029/2018gc007584

Piper, J. D. A. (1975, 03). The palaeomagnetism of precambrian igneous and sedimentary rocks of the orange river belt in south africa and south west africa. *Geophysical Journal International*, *40*, 313-344. doi: 10.1111/j.1365-246x.1975.tb04135.x

Salminen, J., Hanson, R., Evans, D. A., Gong, Z., Larson, T., Walker, O., ... Ernst, R. (2018, 10). Direct mesoproterozoic connection of the congo and kalahari cratons in proto-africa: Strange attractors across supercontinental cycles. *Geology*, *46*, 1011-1014. doi: 10.1130/g45294.1

Schneider, T., Borg, G., Becker, T., Hilken, U., Hansen, B., & Weber, K. (2004, 01). New u-pb zircon ages of the nückopf formation and their significance for the mesoproterozoic event in namibia. *Communications - Geological Survey of Namibia*, *13*, 63-74.

Torsvik, T. H., & Cocks, L. R. M. (2011). The palaeozoic palaeogeography of central gondwana. *Geological Society, London, Special Publications*, *357*, 137-166. doi: 10.1144/sp357.8

Torsvik, T. H., & Van der Voo, R. (2002, 12). Refining gondwana and pangea palaeogeography: estimates of phanerozoic non-dipole (octupole) fields. *Geophysical Journal International*, *151*, 771-794. doi: 10.1046/j.1365-246x.2002.01799.x

van Schijndel, V., Cornell, D. H., Frei, D., Simonsen, S. L., & Whitehouse, M. J. (2014, 01). Crustal evolution of the rehoboth province from archaean to mesoproterozoic times: Insights from the rehoboth basement inlier. *Precambrian Research*, *240*, 22-36. doi: 10.1016/j.precamres.2013.10.014

Ziegler, U. R. F., & Stoessel, G. F. U. (1990). Isotope geology and geochemistry of the rehoboth basement inlier, namibia/s.w. africa; a multimethod case history. *Bulletin der Vereinigung Schweizerischer Petroleum-Geologen und -Ingenieure*, *56*, 13-33.

Appendix

		Partial unfolding of bedding corrections					David Evans, December 6, 2006				
				referenced to mag N			In situ vector		In situ vector		
Site name	Site Var'n	In situ D	In situ I	Bed RHS	Bed dip	Weight	radians D	radians I	N	E	U
Vuong's fold test: HTO (ChRM)							0	0	1	0	0
T1	0	196.3	-23.1	278	11	0	3.426081	-0.40317	-0.88285	-0.25816	0.392337
T2 basalt	0	229.5	-61.8	271.8	36	0	4.005531	-1.07861	-0.3069	-0.35933	0.881303
T3	0	210.6	-29.5	273.4	36	0	3.675663	-0.51487	-0.74915	-0.44305	0.492424
T4	0	201.2	-16.3	46.6	23	0	3.511602	-0.28449	-0.89485	-0.34709	0.280667
V1	0	209.3	-45.4	282.8	49	0	3.652974	-0.79238	-0.61233	-0.34362	0.712026
							0	0	1	0	0
Rotate CC	**20**						0	0	1	0	0
T1	0	176.3	-23.1	278	11	1	3.077015	-0.40317	-0.9179	0.059358	0.392337
T2 basalt	0	209.5	-61.8	271.8	36	1	3.656465	-1.07861	-0.41129	-0.2327	0.881303
T3	0	190.6	-29.5	273.4	36	1	3.326598	-0.51487	-0.8555	-0.1601	0.492424
T4	0	181.2	-16.3	46.6	23	1	3.162537	-0.28449	-0.95959	-0.0201	0.280667
V1	0	209.3	-45.4	282.8	49	1	3.652974	-0.79238	-0.61233	-0.34362	0.712026

Do not delete these rows					Do not delete these rows				Do not delete these rows		

SUMMARY TABLE OF PARTIAL UNFOLDING

% unfold		mean D	mean I	n	R	k	a95				
-20											
-10											
0		190.5	-35.8	5	4.713	13.9	21.2	**IN SITU**			
10		190.5	-33.5	5	4.753	16.2	19.6				
20		190.5	-31.2	5	4.786	18.7	18.2				
30		190.6	-28.9	5	4.811	21.1	17.0				
40		190.6	-26.6	5	4.827	23.2	16.2				
50		190.7	-24.4	5	4.836	24.4	15.8			k2/k1	
60		190.8	-22.1	5	4.837	24.5	15.8			1.76347	
70		190.9	-19.8	5	4.830	23.5	16.1				
80		191.0	-17.5	5	4.815	21.7	16.8				
90		191.1	-15.1	5	4.793	19.3	17.8			k2/k1	
100		191.3	-12.8	5	4.763	16.9	19.2	**TILT-CORRECTED**		1.21478	
110		189.9	-12.5	5	8.533	-1.1	#NUM!				
120		190.1	-10.4	5	8.459	-1.2	#NUM!				
130		190.3	-8.3	5	8.374	-1.2	#NUM!				
140		190.6	-6.2	5	8.278	-1.2	#NUM!				
150		190.9	-4.0	5	8.170	-1.3	#NUM!				

n	**F-table (2n-2)**	**p=0.05**	**p=0.01**	**(from Fisher+87, p.219, using the half-p-value tables in Appendix A5)**
3	4	9.605	23.15	
4	6	5.82	11.07	
5	8	4.433	7.496	
6	10	3.717	5.847	
7	12	3.277	4.906	
13	24	2.269	2.967	

Figure 1: Excel table for the fold test on V19V and V19T sample suites.

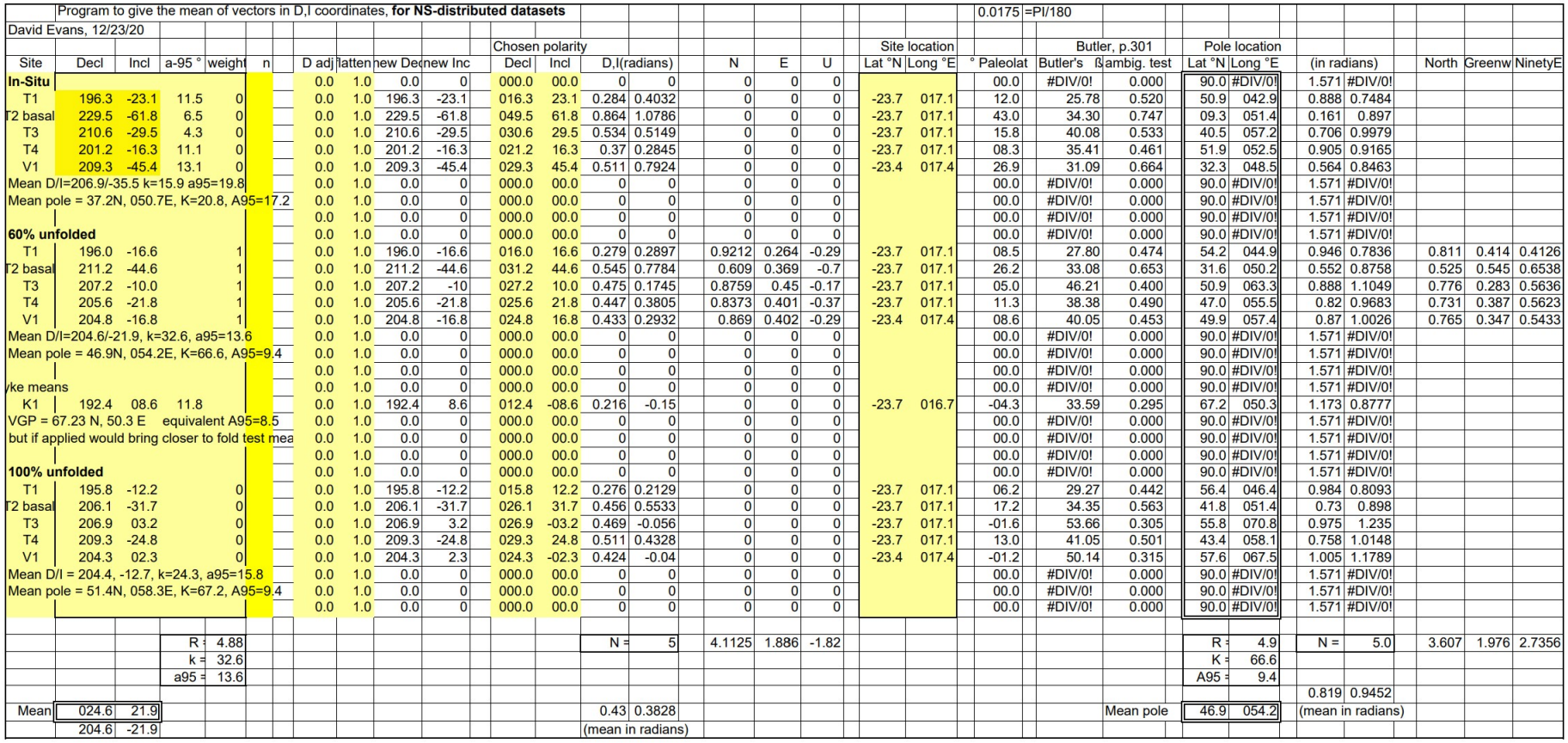

	Program to give the mean of vectors in D,I coordinates, **for NS-distributed datasets**																		0.0175	=PI/180										
David Evans, 12/23/20																														
											Chosen polarity							Site location			Butler, p.301			Pole location						
Site	Decl	Incl	a-95 °	weight	n	D adj	flatten	new Dec	new Inc	Decl	Incl	D,I(radians)		N	E	U	Lat °N	Long °E	° Paleolat	Butler's	ß ambig. test	Lat °N	Long °E	(in radians)		North	Greenw	NinetyE
In-Situ						0.0	1.0	0.0	0	000.0	00.0	0	0	0	0	0			00.0	#DIV/0!	0.000	90.0	#DIV/0!	1.571	#DIV/0!				
T1	196.3	-23.1	11.5	0		0.0	1.0	196.3	-23.1	016.3	23.1	0.284	0.4032	0	0	0	-23.7	017.1	12.0	25.78	0.520	50.9	042.9	0.888	0.7484				
T2 basal	229.5	-61.8	6.5	0		0.0	1.0	229.5	-61.8	049.5	61.8	0.864	1.0786	0	0	0	-23.7	017.1	43.0	34.30	0.747	09.3	051.4	0.161	0.897				
T3	210.6	-29.5	4.3	0		0.0	1.0	210.6	-29.5	030.6	29.5	0.534	0.5149	0	0	0	-23.7	017.1	15.8	40.08	0.533	40.5	057.2	0.706	0.9979				
T4	201.2	-16.3	11.1	0		0.0	1.0	201.2	-16.3	021.2	16.3	0.37	0.2845	0	0	0	-23.7	017.1	08.3	35.41	0.461	51.9	052.5	0.905	0.9165				
V1	209.3	-45.4	13.1	0		0.0	1.0	209.3	-45.4	029.3	45.4	0.511	0.7924	0	0	0	-23.4	017.4	26.9	31.09	0.664	32.3	048.5	0.564	0.8463				
Mean D/I=206.9/-35.5 k=15.9 a95=19.8						0.0	1.0	0.0	0	000.0	00.0	0	0	0	0	0			00.0	#DIV/0!	0.000	90.0	#DIV/0!	1.571	#DIV/0!				
Mean pole = 37.2N, 050.7E, K=20.8, A95=17.2						0.0	1.0	0.0	0	000.0	00.0	0	0	0	0	0			00.0	#DIV/0!	0.000	90.0	#DIV/0!	1.571	#DIV/0!				
						0.0	1.0	0.0	0	000.0	00.0	0	0	0	0	0			00.0	#DIV/0!	0.000	90.0	#DIV/0!	1.571	#DIV/0!				
60% unfolded						0.0	1.0	0.0	0	000.0	00.0	0	0	0	0	0			00.0	#DIV/0!	0.000	90.0	#DIV/0!	1.571	#DIV/0!				
T1	196.0	-16.6		1		0.0	1.0	196.0	-16.6	016.0	16.6	0.279	0.2897	0.9212	0.264	-0.29	-23.7	017.1	08.5	27.80	0.474	54.2	044.9	0.946	0.7836	0.811	0.414	0.4126
T2 basal	211.2	-44.6		1		0.0	1.0	211.2	-44.6	031.2	44.6	0.545	0.7784	0.609	0.369	-0.7	-23.7	017.1	26.2	33.08	0.653	31.6	050.2	0.552	0.8758	0.525	0.545	0.6538
T3	207.2	-10.0		1		0.0	1.0	207.2	-10	027.2	10.0	0.475	0.1745	0.8759	0.45	-0.17	-23.7	017.1	05.0	46.21	0.400	50.9	063.3	0.888	1.1049	0.776	0.283	0.5636
T4	205.6	-21.8		1		0.0	1.0	205.6	-21.8	025.6	21.8	0.447	0.3805	0.8373	0.401	-0.37	-23.7	017.1	11.3	38.38	0.490	47.0	055.5	0.82	0.9683	0.731	0.387	0.5623
V1	204.8	-16.8		1		0.0	1.0	204.8	-16.8	024.8	16.8	0.433	0.2932	0.869	0.402	-0.29	-23.4	017.4	08.6	40.05	0.453	49.9	057.4	0.87	1.0026	0.765	0.347	0.5433
Mean D/I=204.6/-21.9, k=32.6, a95=13.6						0.0	1.0	0.0	0	000.0	00.0	0	0	0	0	0			00.0	#DIV/0!	0.000	90.0	#DIV/0!	1.571	#DIV/0!				
Mean pole = 46.9N, 054.2E, K=66.6, A95=9.4						0.0	1.0	0.0	0	000.0	00.0	0	0	0	0	0			00.0	#DIV/0!	0.000	90.0	#DIV/0!	1.571	#DIV/0!				
						0.0	1.0	0.0	0	000.0	00.0	0	0	0	0	0			00.0	#DIV/0!	0.000	90.0	#DIV/0!	1.571	#DIV/0!				
/ke means						0.0	1.0	0.0	0	000.0	00.0	0	0	0	0	0			00.0	#DIV/0!	0.000	90.0	#DIV/0!	1.571	#DIV/0!				
K1	192.4	08.6	11.8			0.0	1.0	192.4	8.6	012.4	-08.6	0.216	-0.15	0	0	0	-23.7	016.7	-04.3	33.59	0.295	67.2	050.3	1.173	0.8777				
VGP = 67.23 N, 50.3 E equivalent A95=8.5						0.0	1.0	0.0	0	000.0	00.0	0	0	0	0	0			00.0	#DIV/0!	0.000	90.0	#DIV/0!	1.571	#DIV/0!				
but if applied would bring closer to fold test mea						0.0	1.0	0.0	0	000.0	00.0	0	0	0	0	0			00.0	#DIV/0!	0.000	90.0	#DIV/0!	1.571	#DIV/0!				
						0.0	1.0	0.0	0	000.0	00.0	0	0	0	0	0			00.0	#DIV/0!	0.000	90.0	#DIV/0!	1.571	#DIV/0!				
100% unfolded						0.0	1.0	0.0	0	000.0	00.0	0	0	0	0	0			00.0	#DIV/0!	0.000	90.0	#DIV/0!	1.571	#DIV/0!				
T1	195.8	-12.2		0		0.0	1.0	195.8	-12.2	015.8	12.2	0.276	0.2129	0	0	0	-23.7	017.1	06.2	29.27	0.442	56.4	046.4	0.984	0.8093				
T2 basal	206.1	-31.7		0		0.0	1.0	206.1	-31.7	026.1	31.7	0.456	0.5533	0	0	0	-23.7	017.1	17.2	34.35	0.563	41.8	051.4	0.73	0.898				
T3	206.9	03.2		0		0.0	1.0	206.9	3.2	026.9	-03.2	0.469	-0.056	0	0	0	-23.7	017.1	-01.6	53.66	0.305	55.8	070.8	0.975	1.235				
T4	209.3	-24.8		0		0.0	1.0	209.3	-24.8	029.3	24.8	0.511	0.4328	0	0	0	-23.7	017.1	13.0	41.05	0.501	43.4	058.1	0.758	1.0148				
V1	204.3	02.3		0		0.0	1.0	204.3	2.3	024.3	-02.3	0.424	-0.04	0	0	0	-23.4	017.4	-01.2	50.14	0.315	57.6	067.5	1.005	1.1789				
Mean D/I = 204.4, -12.7, k=24.3, a95=15.8						0.0	1.0	0.0	0	000.0	00.0	0	0	0	0	0			00.0	#DIV/0!	0.000	90.0	#DIV/0!	1.571	#DIV/0!				
Mean pole = 51.4N, 058.3E, K=67.2, A95=9.4						0.0	1.0	0.0	0	000.0	00.0	0	0	0	0	0			00.0	#DIV/0!	0.000	90.0	#DIV/0!	1.571	#DIV/0!				
						0.0	1.0	0.0	0	000.0	00.0	0	0	0	0	0			00.0	#DIV/0!	0.000	90.0	#DIV/0!	1.571	#DIV/0!				
			R =	4.88								N =	5	4.1125	1.886	-1.82						R =	4.9	N =	5.0	3.607	1.976	2.7356
			k =	32.6																		K =	66.6					
			a95 =	13.6																		A95 =	9.4					
																								0.819	0.9452			
Mean	024.6	21.9										0.43	0.3828								Mean pole	46.9	054.2	(mean in radians)				
	204.6	-21.9										(mean in radians)																

Figure 2: Excel table for the calculation of VGPs.

Sample	ID	NRM	LN2	100	150	230	300	370	430	490	530	560	580	600	615	630	640	650	655	660	665	670	673	676	678	680	682	684	686	688	Origin	Geographic Declination	Geographic Inclination	Stratigraphic Declination	Stratigraphic Inclination	MAD (6 degree cutoff)
A	LTH	x	x	x	x	x	x	x	x																							49.9	4.7	49.8	-3.6	7.1
	HTO																				x	x	x	x	x	x	x	x	x	x	x	198	-29.2	197.2	-18.3	1.6
B	LTH		x	x																												48.9	-19.9	52.2	-28.3	0.7
	LT2			x	x	x	x	x	x																							26.8	23.6	25.9	13.5	12.1
	HTO																				x	x	x	x	x	x	x	x	x	x	x	197.4	-24.6	196.8	-13.8	0.9
C	LTH	x	x	x	x																											52.7	-4.9	54.1	-12.7	10
	HTO																				x	x	x	x	x	x	x	x	x	x	x	197.3	-20.6	196.8	-9.7	1
D	LTH		x	x																												72.9	-23.3	77.5	-27.9	4.8
	LT2			x	x	x	x	x	x	x																						353.9	30.2	355.4	19.7	8.8
	HTO																				x	x	x	x	x	x	x	x	x	x	x	203.9	-20.2	203.1	-9.6	1
E	LTH		x	x	x																											59.4	0	59.8	-6.8	18
	LT2				x	x	x	x	x	x	x	x																				293.3	31.4	299.4	27.7	10.3
	HTO																						x	x	x	x	x	x	x	x	x	191.7	-44.6	191.2	-33.6	1.5
F	LTH		x	x	x																											53.2	-18.9	56.6	-26.4	4.4
	LT2				x	x	x	x	x																							37.9	6.6	37.4	-2.9	2.5
	HTO																						x	x	x	x	x	x	x	x	x	191.6	4.9	191.8	15.9	1.4
G	LTH		x	x	x																											24.3	-27.8	27	-3.7	13.9
	LT2					x	x	x	x	x																						346.7	50.3	350.6	39.5	7.3
	HTO																						x	x	x	x	x	x	x	x	x	193.7	-26.7	193.3	-15.7	0.8

Figure 3: LSQ Excel table for sample site V19T1.

Sample	ID	NRM	LN2	100	150	230	300	370	430	490	530	560	580	600	615	630	640	650	655	660	665	670	675	680	685	690	695	Origin	Geographic Declination	Geographic Inclination	Stratigraphic Declination	Stratigraphic Inclination	MAD (6 degree cutoff)
A																																	
	HTO																				x	x	x	x	x	x	x	x	241	-68	206	-39.6	0.3
B																																	
	HTO																					x	x	x	x	x	x	x	230	-56	210	-26.5	0.7
C																																	
	HTO																					x	x	x	x	x	x	x	229	-64	204	-33.2	0.4
D																																	
	HTO																					x	x	x	x	x	x	x	230	-65	205	-34.3	0.4
E																																	
	HTO																						x	x	x	x	x	x	235	-59	211	-30.9	0.5
F																																	
	HTO																						x	x	x	x	x	x	221	-67	199	-34.9	0.5
G																																	
	HTO																					x	x	x	x	x	x	x	228	-72	199	-39.6	0.4
H																																	
	HTO																					x	x	x	x	x	x	x	224	-43	212	-13.7	1.4

Figure 4: LSQ Excel table for sample site V19T2.

Sample	ID	NRM	LN2	100	150	230	300	370	430	490	530	560	580	600	615	630	640	650	655	660	665	670	673	676	678	680	682	684	686	688	Origin	Geographic Declination	Geographic Inclination	Stratigraphic Declination	Stratigraphic Inclination	MAD (6 degree cutoff)
A	LTH	x	x	x	x																											38.4	-36	70.5	-60	11.2
	HTO																				x	x	x	x	x	x	x	x	x	x	x	209	-35	205	-1.4	1.8
B																																				
	HTO																					x	x	x	x	x	x	x	x	x	x	210	-28	207	4.6	1.8
C	LTH		x	x	x																											33	-39	67.5	-65	2.2
	HTO																						x	x	x	x	x	x	x	x	x	202	-31	200	3.1	1.5
D																																				
	HTO																							x	x	x	x	x	x	x	x	215	-30	211	2.1	1.2
E																																				
	HTO																							x	x	x	x	x	x	x	x	210	-34	206	-1.1	1.9
F	LTH	x	x	x	x																											308	-30	282	-44	9
	HTO																						x	x	x	x	x	x	x	x	x	210	-23	208	9.6	1.5
G																																				
	HTO																						x	x	x	x	x	x	x	x	x	216	-25	213	5.7	1.4

Figure 5: LSQ Excel table for sample site V19T3.

Sample	ID	NRM	LN2	100	150	230	300	370	430	490	530	560	580	600	615	630	640	650	655	660	665	670	673	676	678	680	682	684	686	688	Origin	Geographic Declination	Geographic Inclination	Stratigraphic Declination	Stratigraphic Inclination	MAD (6 degree cutoff)
A	LTH		x	x	x																										29	-21.4	22.5	-13	8.7
	HTO																				x	x	x	x	x	x	x	x	x	x	215.2	-22.1	225.3	-24.7	1.9
B	LMT	x	x	x	x	x	x	x	x																						82.4	3.9	81.5	-9.6	5
	HTO																				x	x	x	x	x	x	x	x	x	x	178.1	-2.4	181.1	-19.2	3.4
C	LMT	x	x	x			x	x	x																						36.1	32.4	51.4	33.6	15.6
	HTO																				x		x	x		x	x		x	x	210.3	-36.8	228.7	-39.8	6.3
D	LTH	x	x	x																											358.1	-29.6	353	-11.3	8.5
	LT2				x	x	x	x	x																						353.6	-25.5	4.1	42.8	4
	HTO																				x	x	x	x	x	x	x	x	x	x	198	-9.8	203.6	-20	1.7
E	LMT			x	x	x	x	x	x																						43.7	37.9	60.8	35.9	10.3
	HTO																				x	x	x	x	x	x	x	x	x	x	194.4	-4.4	198.1	-16.1	1.8
F	LTH		x	x	x	x																									345.5	68.2	66.7	79.5	8.4
	LT2						x	x	x	x																					352.9	79.4	114.1	74.5	1.2
	HTO																				x	x	x	x	x	x	x	x	x	x	202.1	-21.5	212.5	-29.6	1.2
G	LMT	x		x	x	x	x	x	x																						344.4	63.7	43.4	78.5	9.6
	HTO																				x	x	x	x	x	x	x	x	x	x	205.2	-20.6	215.2	-27.6	2.1
H	LMT		x	x	x	x	x	x	x																						4.4	49.1	34.1	60.6	5.2
	HTO																				x	x	x	x	x	x	x	x	x	x	209.3	10.8	214.9	-17	1.6

Figure 6: LSQ Excel table for sample site V19T4.

Sample	ID	NRM	LN2	100	150	230	300	370	430	490	530	560	580	600	615	630	640	650	655	660	665	670	673	676	678	680	682	684	686	688	Origin	Geographic Declination	Geographic Inclination	Stratigraphic Declination	Stratigraphic Inclination	MAD (6 degree cutoff)
A	LTH	x	x	x																												305.2	-33.8	267.3	-37	2.4
	LT2				x	x	x	x	x	x	x	x	x																			329.6	-26.9	290.8	-51.9	5.9
	HTO																							x	x	x	x	x	x	x	x	203	-44.2	200.1	4.3	4.1
B	LMT	x	x	x	x	x	x	x	x	x	x	x	x	x																		110.4	54.8	58	36.5	8.3
	HTO																								x	x	x	x	x	x	x	200.2	-15.2	201.4	33.4	6
C	LMT										x	x	x	x	x																	248.2	-22.1	244.8	9.7	7.2
	HTO																							x	x	x	x	x	x	x	x	212.5	-43.2	207.1	3.9	1.6
D	LMT							x	x	x	x	x	x	x																		258.9	-19.5	252.8	4	11.1
	HTO																								x	x	x	x	x	x	x	206.9	-38.9	203.9	9.1	1.9
E	LMT					x	x	x	x	x	x	x																				272.1	-59.9	227.5	-29.4	5.1
	HTO																							x	x	x	x	x	x	x	x	198.5	-59.4	195.8	-10.6	2.1
F	LMT					x	x	x	x	x	x	x		x	x	x	x	x	x	x	x	x	x	x								260.6	-40.6	238.7	-12.4	16.3
	HTO																									x	x	x	x	x	x	225.5	-51.1	212.8	-6.5	2.9
G	LMT					x	x	x	x	x	x	x	x																			288.1	-34	258.7	-25.2	6.5
	HTO																										x	x	x	x	x	226.8	-61.9	208.8	-16.5	3.5
H	LMT					x	x	x	x	x	x																					289.7	20	302.4	8	6.9
	HTO																									x	x	x	x	x	x	268.1	-4.2	269.9	8.2	1

Figure 7: LSQ Excel table for sample site V19V1.

Sample	ID	NRM	LN2	100	150	230	300	370	430	470	500	515	525	535	545	550	555	575	580	Origin	Geographic Declination	Geographic Inclination	Stratigraphic Declination	Stratigraphic Inclination	MAD (6 degree cutoff)
A	LTO						x	x	x	x	x	x	x	x	x	x	x	x	x	x	180	37	180	37	0.4
B	LTO						x	x	x	x	x	x	x	x	x	x	x	x	x	x	190	23.7	190	23.7	0.6
C	LTO			x	x	x	x	x	x	x	x	x	x	x	x	x	x	x	x	x	199	1.2	199	1.2	1.7
D	LTO					x	x	x	x	x	x	x	x	x	x	x	x	x	x	x	204	3.8	204	3.8	1.8
E	LTO					x	x	x	x	x	x	x	x	x	x	x	x	x	x	x	196	5.1	196	5.1	0.9
F	LTO					x	x	x	x	x	x	x	x	x	x	x	x	x	x	x	195	2.4	195	2.4	1
G	LTO						x	x	x	x	x	x	x	x	x	x	x	x	x	x	195	1.6	195	1.6	0.9
H	LTO						x	x	x	x	x	x	x	x	x	x	x	x	x	x	176	-5.8	176	-5.8	2

Figure 8: LSQ Excel table for sample site C19K1.

Sample	ID	NRM	LN2	100	150	230	300	370	430	470	500	515	525	535	545	550	555	560	565	570	575	580	Origin	Geographic I	Geographic I	Stratigraphic	Stratigraphic	MAD (6 degr
A	LTO					x	x	x	x	x	x	x	x	x	x	x	x	x	x	x	x	x	x	184	25			3.8
B	LTO					x	x	x	x	x	x	x	x	x	x	x	x	x	x	x	x	x	x	177	33.9			2.8
C	LTO					x	x	x	x	x	x	x	x	x	x	x	x	x	x	x	x	x	x	220	-50			3.8
D	LTO					x	x	x	x	x	x	x	x	x	x	x	x	x	x	x	x	x	x	223	-72			4.3
E	LTO					x	x	x	x	x	x	x	x	x	x	x	x	x	x	x	x	x	x	187	-51			5.6
F	LTO					x	x	x	x	x	x	x	x	x	x	x	x	x	x	x	x	x	x	177	-59			3
G	LTO					x	x	x	x	x	x	x	x	x	x	x	x	x	x	x	x	x	x	151	-33			4.4
H	LTO						x	x	x	x	x	x	x	x	x	x	x	x	x	x	x	x	x	118	-18			3.8

Figure 9: LSQ Excel table for sample site C19K2.

Sample	ID	NRM	LN2	100	150	230	300	370	430	470	500	515	525	535	545	550	555	560	565	570	575	580	Origin	Geogral	Geogral	Stratigr	Stratigr	MAD (6
A	LTC					x	x	x	x															11.9	-24			4.6
	MTC															x	x	x	x	x	x	x		52	-36			26.2
	HPL															x	x	x	x	x	x	x	x	105	34.4			37.8
	SEP																				x	x	x	5.2	22.7			14.8
B	LTH				x	x	x	x																4.9	-34			8
	HTO											x	x	x	x	x	x	x	x	x	x	x	x	29.9	-35			8
C	LTC			x	x	x																		336	-17			9.1
	MTC								x	x	x			x	x		x	x	x			x	x	45	17.1			9.6
D	LTC				x	x	x	x																347	28.2			6
	MTC							x	x	x	x													339	-25			6.7
E	LTC				x	x	x	x																27.6	-3.4			11.2
	MTC								x			x				x								5.6	1.3			6.4
	HPL								x			x				x							x	268	77.5			5.6
	SEP															x							x	70.9	14.1			0
F	LTC					x	x	x	x	x	x	x												195	-64			8.3
	MTC														x	x	x			x				218	50.7			10.8
	HPL														x	x	x			x			x	346	27.1			3.6
	SEP																x			x			x	205	56.6			1.1
G	LTC				x	x	x	x	x	x	x	x	x	x	x	x	x	x	x	x	x	x	x	269	5.3			4.1
H	LTC			x	x	x	x																	17.8	-54			5.8
	MTC								x	x	x		x					x			x			30.1	-64			9.4
	HPL								x	x	x		x					x			x			82.5	18.5			32.1
	SEP																				x		x	77.6	-62			0

Figure 10: LSQ Excel table for sample site C19K3.

Sample	ID	NRM	LN2	100	150	230	300	370	430	470	500	515	525	535	545	550	555	575	580	Origin	Geographic Declination	Geographic Inclination	Stratigraphic Declination	Stratigraphic Inclination	MAD (6 degree cutoff)
A	LTO			x	x	x	x	x	x	x	x	x	x	x	x	x	x	x	x	x	25.3	68	25.3	68	4.8
B	LTO						x	x	x	x	x	x	x	x	x	x	x	x	x	x	60	42	60	42	1.9
C	LTO						x	x	x	x	x	x	x	x	x	x	x	x	x	x	66.8	64.7	66.8	64.7	0.7
D	LTO						x	x	x	x	x	x	x	x	x	x	x	x	x	x	49.3	22.9	49.3	-22.9	2.5
E	LTO						x	x	x	x	x	x	x	x	x	x	x	x	x	x	43.8	-67.6	34.8	-67.5	1.5
F	LTO						x	x	x	x	x	x	x	x	x	x	x	x	x	x	48.1	-17.6	48.1	-17.6	2.1
G	LTO						x	x	x	x	x	x	x	x	x	x	x	x	x	x	42.7	-24.5	42.7	-24.5	2.6
H	LTO						x	x	x	x	x	x	x	x	x	x	x	x	x	x	26.4	-54.4	26.4	-54.4	1.3

Figure 11: LSQ Excel table for sample site C19K4.

Sample	ID	NRM	LN2	100	150	230	300	370	430	470	500	515	525	535	545	550	555	560	565	570	575	580	Origin	Geographic Declination	Geographic Inclination	Stratigraphic Declination	Stratigraphic Inclination	MAD (6 degree cutoff)
A	LTC			x	x	x																		41.9	1.9			3.4
	MTC						x	x	x	x	x	x	x	x	x	x	x	x	x	x	x	x	x	342	4.3			1.2
B	LTC	x	x	x	x	x																		21	3.8			12.4
	MTC						x	x	x	x	x	x	x	x	x	x	x	x	x	x	x	x	x	341	-0.9			1.3
C	LTO	x	x	x	x	x	x	x	x	x	x	x	x	x	x	x	x	x	x	x	x	x	x	346	-9.5			3.5
D	LTO						x	x	x	x	x	x	x	x	x	x	x	x	x	x	x	x	x	291	22.5			1.5
E	LTC				x	x	x	x	x	x	x													11.9	0.9			6.4
	MTC											x	x	x	x	x	x	x	x	x	x	x	x	309	25.9			7.9
F	LTC						x	x	x	x	x	x												26	34.7			5.7
	MTC												x					x	x				x	356	47.1			4.1
G	LTC		x		x	x																		9.5	-16			4.6
	MTC						x	x	x	x	x	x	x	x	x	x	x	x	x	x	x	x		320	42.9			8
	HPL						x	x	x	x	x	x	x	x	x	x	x	x	x	x	x	x	x	116	43.5			26.7
	SEP																		x	x				321	44.3			3.1
H	LTC		x	x	x	x																		319	-16			9.6
	MTC									x	x	x	x			x	x							281	64.8			7.1
	HPL									x	x	x	x			x	x						x	46.5	12.6			42
	SEP															x	x						x	305	51.6			2.6

Figure 12: LSQ Excel table for sample site C19K5.

Sample	ID	NRM	LN2	100	150	230	300	370	430	470	500	515	525	535	545	550	555	560	565	570	575	580	Origin	Geographic	Geographic	Stratigraph	Stratigraph	MAD (6 de
A	LTC			x	x	x	x	x															x	85.9	59.1			3.3
B	LTC		x	x	x	x	x	x																356.1	-25.9			15.5
	MTC								x	x	x	x	x	x	x	x	x	x						44.5	13.6			15.3
	HPL								x	x	x	x	x	x	x	x	x	x						323	-42.2			34.2
	SEP																	x					x	69	-20.9			0
C	LTC		x	x	x																			20.5	0.8			3.6
	MTC					x	x	x																131.1	35.5			6.1
	HPL					x	x	x																293.7	54.2			18.5
	SEP							x															x	60.4	23.8			0
D	LTC				x	x	x	x																115.6	52.2			8.7
	HPL				x	x	x	x															x	57.9	-26.9			36.1
	SEP							x															x	67.3	60.4			0
E	LTC			x	x		x																	92.4	-33.1			9.3
	HPL							x	x	x	x	x												82.7	-15.7			33.9
	SEP											x											x	46.9	31.3			0
F	LTC		x	x	x																			118.1	-58.6			7.1
	MTC						x	x	x	x	x													55.6	28.7			17.7
	HPL						x	x	x	x	x												x	62.5	14.6			10.3
	SEP										x												x	75.5	18.1			0
G	LTC		x	x	x																			344.1	-22.5			10.6
	MTC					x	x	x																63.5	25.8			3
	HPL					x	x	x															x	336.2	-6			5.5
	SEP							x															x	259.2	57.7			0
H	LTC	x	x	x	x	x	x																	338.2	-3.4			20.6
	HPL	x	x	x	x	x	x																x	19	49.8			8.1
	SEP						x																x	31.9	57.4			0

Figure 13: LSQ Excel table for sample site C19K6.

Sample	ID	NRM	LN2	100	150	230	300	370	430	470	500	515	525	535	545	550	555	560	565	570	575	580	Origin	Geograp	Geograp	Stratigra	Stratigra	MAD (6
A	LTO						x	x	x	x														321	14.2			12.4
	HPL						x	x	x	x													x	206	62			18.1
	SEP									x													x	23	20.5			0
C	LTC	x	x	x	x	x	x	x	x	x	x	x	x	x	x	x	x	x	x	x	x	x	x	49.6	44.8			1.1
D	LTC	x	x	x	x	x	x	x															x	269	69.1			3
E	LTC	x	x	x	x	x	x	x															x	318	50.5			5.4
G	LTC	x	x	x	x	x	x	x	x	x	x	x	x	x	x	x	x	x	x	x	x	x	x	279	-8.4			2.2
H	LTC		x	x	x	x	x	x	x	x	x	x	x	x	x	x	x	x	x	x	x	x	x	266	-9.8			3.1

Figure 14: LSQ Excel table for sample site C19K7.